

Confined Vortex Surface and Irreversibility. 2. Hyperbolic Sheets and Turbulent statistics

Alexander Migdal

*Department of Physics, New York University
726 Broadway, New York, NY 10003*

We continue the study of Confined Vortex Surfaces (CVS) that we introduced in the previous paper. We classify the solutions of the CVS equation and find the analytical formula for the velocity field for arbitrary background strain eigenvalues in the stable region. The vortex surface cross-section has the form of four symmetric hyperbolic sheets with a simple equation $|y||x|^{\mu} = 1$ in each quadrant of the tube cross-section (xy plane).

We use the dilute gas approximation for the vorticity structures in a turbulent flow, assuming their size is much smaller than the mean distance between them. We vindicate this assumption by the scaling laws for the surface shrinking to zero in the extreme turbulent limit. We introduce the Gaussian random background strain for each vortex surface as an accumulation of a large number of small random contributions coming from other surfaces far away. We compute this self-consistent background strain, relating the variance of the strain to the energy dissipation rate.

We find a universal asymmetric distribution for energy dissipation. An unexpected new phenomenon is a multifractal distribution of the shape of the profile of the vortex tube in the xy plane. Its fractal dimension is a random variable distributed between $\frac{1}{3}$ and $\frac{2}{3}$. This phenomenon naturally leads to the so-called multi-fractal scaling for the moments of velocity difference $v(\vec{r}_1) - v(\vec{r}_2)$. We argue that the phenomenological relations for these moments suggested in a recent paper by Sreenivasan and Yakhot are consistent with the CVS theory. We reinterpret their renormalization parameter $\alpha \approx 0.95$ in the Bernoulli law $p = -\frac{1}{2}\alpha\bar{v}^2$ as a probability to find no vortex surface at a random point in space.

1. Introduction

The ultimate goal of turbulence studies is to solve the Navier-Stokes equations and determine how and why the solution covers some manifold rather than staying unique given initial data and boundary conditions.

We also need to understand why it is irreversible even in the limit of zero viscosity when the Navier-Stokes equations formally become the Euler equation corresponding to the reversible Hamiltonian system with conserved energy.

Once we know why and how the solution covers some manifold, we would like to know its parameters and the invariant measure.

The first obstacle to overcome on this path is to understand the irreversibility of the Navier-Stokes dynamics in a limit when the viscosity goes to zero at fixed energy dissipation.

We know (or at least we assume) that the vortex structures in this extreme turbulent flow collapse into thin clusters in physical space. Snapshots of vorticity in

numerical simulations show a collection of tube-like structures relatively sparsely distributed in space.

We know such 2D structures in the Euler dynamics: these are vortex surfaces. Vorticity collapses into a thin boundary layer around the surface which is moving in a self-generated velocity field. Such motion is known to be unstable against the Kelvin-Helmholtz instabilities, which undermines the whole idea of random vortex surfaces.

However, the exact solutions of the Navier-Stokes equations discovered in the previous century by Burgers and Townsend^{1,2} show stable planar sheets with Gaussian profile of the vorticity in the normal direction. This nice Gaussian solution is not the most general one; it takes some tuning parameters in the background flow.

The recent research^{3,4} revealed that the Burgers-Townsend regime required vanishing normal velocity, vanishing strain in the direction of the tangent velocity gap, plus the negative value of the normal component of the strain.

Abstracting from these observations, we conjectured⁵ that the stability condition of the vortex surface is given by three equations

$$\vec{v} \cdot \vec{\sigma} = 0; \quad (1)$$

$$\hat{S} \cdot \Delta \vec{v} = 0; \quad (2)$$

$$S_{nn} = \vec{\sigma} \cdot \hat{S} \cdot \vec{\sigma} < 0 \quad (3)$$

The first condition is simply a statement that the surface is stationary. The second one is an enhanced version of the vanishing eigenvalue requirement. The velocity gap Δv should be a null vector of this zero eigenvalue. This requirement is stronger than $\det \hat{S} = 0$.

With $\vec{\sigma}$ being the local normal vector, the third requirement demands that the strain pushes the fluid towards the surface on both sides.

With negative normal strain and zero strain in the direction of velocity gap, the flow effortlessly slides along the surface on both sides, without leakage and pile-up.

Here is an intuitive explanation of the CVS conditions– they provide the permanent tangential flow around the surface, confining vorticity inside the boundary layer.

Once these requirements are satisfied in the local tangent plane, one could solve the Navier-Stokes equation in the boundary layer and obtain the Gaussian Burgers-Townsend solution, vindicating the stability hypothesis. The error function of the normal coordinate will replace the velocity gap, and the delta function of tangent vorticity will become the Gaussian profile with viscous width.

With the inequality satisfied, this width will be real positive

$$h = \sqrt{\frac{\nu}{-S_{nn}}} \quad (4)$$

It is important to understand that this inequality breaks the reversibility of the

Euler equation: the strain is an odd variable for time reflection, although it is even for space reflection.

This inequality is a dynamic mechanism of the irreversibility of the turbulent flow: the vorticity can collapse only to the surface with negative normal strain.

2. The exact analytic solution

In the first part of this study⁵ we have found the general formula for the velocity field and an equation for this surface.

Let us describe, clarify, and solve this equation before studying the associated turbulent statistics. As we shall see, there is a simple analytic solution to this equation, which we have not noticed in.⁵

2.1. Stationary Vortex Sheets and Double-layer potentials

The steady closed vortex surface \mathcal{S} can be treated within the framework of hydrostatics, as it was recently advocated in our paper.³

In the 3D space inside and outside the surface $\mathcal{S}^\pm : \partial\mathcal{S}^\pm = \mathcal{S}$ there is no vorticity so that the flow can be described by a potential $\Phi(\vec{r})$ with the gap $\Gamma = \Delta\Phi$ on the surface.

This is a well-known double-layer potential from electrostatics.⁶ The potential is given by the Coulomb integral with dipole density Γ plus a background constant strain potential

$$\Phi(\vec{r}) = \frac{1}{2}W_{\alpha\beta}r_\alpha r_\beta - \frac{1}{4\pi} \int_{\mathcal{S}} \Gamma(\vec{r}') d^2\sigma_\alpha(\vec{r}') \partial_\alpha \frac{1}{|\vec{r} - \vec{r}'|}; \quad (5)$$

$$d^2\sigma_\alpha(\vec{r}') = e_{\alpha\beta\gamma} dr_\beta \wedge dr_\gamma; \quad (6)$$

The pressure in each of the domains inside/outside is given by the Bernoulli formula

$$p = -\frac{1}{2} (\partial_\alpha \Phi(\vec{r}))^2 \quad (7)$$

The normal velocity is continuous, as one may readily check. Schematically, this check goes as follows. This formula involves the normal derivative of the Coulomb kernel. Using the Laplace equation on each side of the surface, we reduce the second normal derivative to the minus tangent Laplacian of the Coulomb kernel, which is the same on both sides.

The tangent velocity, on the other hand, has a gap $\Delta\vec{v}$. This gap arises because of the gap in the potential

$$\Gamma = \Phi(\vec{r}^+) - \Phi(\vec{r}^-); \quad \forall \vec{r} \in \mathcal{S}; \quad (8)$$

$$\Delta\vec{v} = \vec{\nabla}\Gamma \quad (9)$$

2.2. CVS Equation for Cylindrical Geometry

In the previous paper,⁵ we considered a cylindrical geometry, where the piecewise harmonic potential has the form

$$\Phi(x, y, z) = \frac{1}{2}ax^2 + \frac{1}{2}by^2 + \frac{1}{2}cz^2 + \mathbf{Re} \phi(\eta); \quad (10)$$

$$a + b + c = 0, a \leq b \leq c; c > 0, a < 0; \quad (11)$$

$$\eta = x + iy; \quad (12)$$

$$\phi(\eta) = \frac{1}{2\pi i} \int d\Gamma(\theta) \log(\eta - C(\theta)); \quad (13)$$

$$v_z = cz; \quad (14)$$

$$V(x, y) = v_x - iv_y = ax - iby + \frac{1}{2\pi i} \int \frac{d\Gamma(\theta)}{\eta - C(\theta)}; \quad (15)$$

Here $C(\theta)$ is a complex periodic function of the angle $\theta \in (0, 2\pi)$ parametrizing the closed loop C . We simplified the notations compared to,⁵ now we denote the ordered eigenvalues of the background strain tensor as a, b, c .

The geometry is as follows. The vortex surface corresponds to the parallel transport of the xy loop C in in the third dimension z . Thus, at some point on the surface, the local tangent frame is

$$\vec{e}_1 = \left(\frac{\mathbf{Re} C'}{|C'|}, \frac{\mathbf{Im} C'}{|C'|}, 0 \right); \quad (16)$$

$$\vec{e}_2 = (0, 0, 1); \quad (17)$$

$$\vec{e}_3 = \left(\frac{\mathbf{Im} C'}{|C'|}, -\frac{\mathbf{Re} C'}{|C'|}, 0 \right) \quad (18)$$

The first two orthogonal vectors define the tangent plane, and the third one $\vec{e}_3 = \vec{e}_1 \times \vec{e}_2$ corresponds to the normal to the surface. Do not confuse the z direction with the normal – this is one of the two tangent directions.

The CVS equations were reduced in⁵ to the complex equation (with V_{\pm} denoting the boundary values at each side of the surface)

$$V_+ (\mathbf{Re} C(\theta), \mathbf{Im} C(\theta)) + V_- (\mathbf{Re} C(\theta), \mathbf{Im} C(\theta)) = 0; \quad (19)$$

The condition of vanishing normal velocity at each side of the steady surface can be reduced to the following real equation

$$\mathbf{Im} C'(\theta) V_- (\mathbf{Re} C(\theta), \mathbf{Im} C(\theta)) = 0; \quad (20)$$

The normal velocity on another side will also vanish in virtue of the CVS equation.

It follows from the CVS equation (19) that one of the two eigenvalues of the local tangent strain at the surface vanishes. This vanishing eigenvalue corresponds to the velocity gap $\Delta V = V_+ - V_- = -2V_-$ as an eigenvector.

The other eigenvalue S_{nn} , corresponding to the eigenvector $\vec{\sigma} = \vec{e}_3$ normal to the surface, is then uniquely fixed by the condition of vanishing trace of the local strain tensor.

The third eigenvalue c corresponds to the eigenvector \vec{e}_2 of our cylindrical tube. Therefore, the normal component of the strain tensor is

$$S_{nn} = -c \quad (21)$$

As the largest c of the three ordered numbers a, b, c with the sum equal to 0 is always positive (unless all three are zero), we have a negative normal strain as required by the stability of the Navier-Stokes equation in the local tangent plane.

This condition does not restrict the background strain tensor, contrary to some of our previous statements. The irreversibility of turbulence manifests itself in the negative sign of the normal strain on the surface, which is true for arbitrary nonzero eigenvalues a, b, c .

The Euler equation is invariant under time reversal, changing the sign of the strain. Without the CVS boundary conditions, both signs of the normal strain would satisfy the stationary Euler equation. Therefore, this CVS vortex sheet represents a dynamical breaking of the time-reversal symmetry.

Out of the two time-reflected solutions of the Euler equation, only the one with the negative normal strain survives. If virtually created as a metastable phase, the other one dissolves in the turbulent flow, but this remains stable.

This irreversibility is not driven by some external forces but rather by internal Navier-Stokes dynamics. The result of this microscopic stability mechanism of the Navier-Stokes dynamics is the CVS boundary conditions added to the ambiguous Euler dynamics of the vortex sheets.

The CVS equations for the cylindrical geometry reduce to the equation (20) for the boundary loop $C(\theta)$ plus a complex equation $V_+(x, y) + V_-(x, y) = 0$ at the loop $(x, y) \in C$.

Consider the complex function involved in this equation

$$F(\eta) = \frac{1}{2\pi i} \int \frac{d\Gamma(\theta)}{\eta - C(\theta)}; \quad (22)$$

It defines two different holomorphic functions: $F_-(\eta)$ inside the loop, $F_+(\eta)$ outside. These two functions are related through the boundary condition

$$F_+(\eta) + F_-(\eta) + 2a\mathbf{Re} \eta - 2i b\mathbf{Im} \eta = 0; \forall \eta \in C; \quad (23)$$

Let us look for the linear solution of Laplace equation inside (constant strain):

$$F_-(\eta) = (p + i q)\eta \quad (24)$$

with some real p, q .

The vanishing normal velocity from the inside leads to the differential equation for $C(\theta)$.

$$\mathbf{Im} ((p + i q)C(\theta) + a\mathbf{Re} C(\theta) - i b\mathbf{Im} C(\theta)) C'(\theta) = 0 \quad (25)$$

This equation is integrable for arbitrary parameters. We shall use two dimensionless parameters α, β to parametrize p, q as follows:

$$p = \frac{b-a}{2} + \frac{c \cos(\beta)}{4\alpha}; \quad (26)$$

$$q = -\frac{c \sin(\beta)}{4\alpha}; \quad (27)$$

The general solution of (25) reads⁷ (up to an arbitrary normalization constant)

$$C(\theta) = e^{i\beta/2}(1 + i\tau)\tau^{\alpha-\frac{1}{2}}; \quad (28)$$

$$\tau = \tan \theta \quad (29)$$

2.3. Parabolic curves

Let us consider positive α first (the parabolic curves).

This solution passes through the origin and it will have no singularity at $\tau = 0$ in case $\alpha = \frac{1}{2} + n, n \in \mathbb{Z}, n \geq 0$.

The case $n = 0$ corresponds to a tilted straight line, Fig.1. This is just a Burgers-Townsend planar vortex sheet. The next cases are already nontrivial Fig.2,3,4.

However, not all positive n are acceptable. For even positive n we have a cusp in a curve, because only positive $r(\theta)$ exist at $\theta \rightarrow 0$. This is clearly visible at $n = 2$ (Fig.3).

For odd positive $n = 2k + 1$ there is a linear relation between x, y at small τ provided $\beta \neq 0$. The slope of the curve $y(x)$ at $x = \pm 0$ is the same.

Higher derivatives are singular, as we have

$$x \sim \tau^{2k+1} \cos\left(\frac{1}{2}\beta\right) \left(1 - \tan\left(\frac{1}{2}\beta\right)\tau\right); \quad (30)$$

$$y \sim \tau^{2k+1} \sin\left(\frac{1}{2}\beta\right) \left(1 + \cot\left(\frac{1}{2}\beta\right)\tau\right); \quad (31)$$

$$y \rightarrow \tan\left(\frac{1}{2}\beta\right) x \left(1 + \frac{2 \operatorname{sign} x}{\sin \beta} \left(\frac{|x|}{\cos\left(\frac{1}{2}\beta\right)}\right)^{\frac{1}{2k+1}}\right); \quad (32)$$

$$\frac{dy}{dx} \rightarrow \tan\left(\frac{1}{2}\beta\right) \text{ at } x \rightarrow \pm 0 \quad (33)$$

As the slopes $\frac{dy}{dx}$ are the same at $x = \pm 0$, the vortex sheet reduces to a plane up to higher-order terms. Thus, the Burgers-Townsend solution, assuming the infinitesimal thickness of the vorticity layer, will still apply here. Ergo, the sheet will be stable at this point and the rest of the surface.

Thus, we have found the discrete parametric family of CVS shapes. It simplifies

in terms of $\tau = \tan \theta$.

$$\eta(\tau) = e^{i\beta/2} (1 + i\tau) \tau^{2k+1}; \quad (34)$$

$$k \in \mathbb{Z}, k \geq 0; \quad (35)$$

$$-\infty < \tau < \infty; \quad (36)$$

We have a conformal map from the τ plane to the plane of $\eta = x + iy$, with our curve C corresponding to the real axis. The physical region outside the loop corresponds to the sector in the lower semiplane, $-\frac{\pi}{(k+1)} < \arg \tau < 0$.

The infinity in the physical space corresponds to infinity in the τ plane.

There are two singular points corresponding to the vanishing derivative $\eta'(\tau) = 0$. This happens at

$$\tau = 0; \quad (37)$$

$$\tau = \frac{i(2k+1)}{2(k+1)}; \quad (38)$$

The first one maps to the origin in the η plane. The second one is in the upper τ semiplane, so it does not affect the inverse function $\tau(\eta)$ in the physical sector of the lower semiplane.

The next step is to find the holomorphic function $F_+(\eta)$ which defines the complex velocity on the external side of the sheet (the internal side has linear velocity $F_-(\eta) = (p + iq)\eta$).

From the CVS equation we get the boundary values, which we express in terms of η, η^*

$$F_+(\eta) = -(p + a - b + iq)\eta + c\eta^*; \quad \forall \eta \in C \quad (39)$$

We have to continue this function from the curve (34) into the part of the complex plane outside of this curve.

Let us express the right side in terms of τ

$$f(\tau) = -(p + a - b + iq)\eta(\tau) + c\tilde{\eta}(\tau) \quad (40)$$

Here $\tilde{\eta}(\tau)$ is the complex conjugate expression for η

$$\tilde{\eta}(\tau) = e^{-i\beta/2} (1 - i\tau) \tau^{2k+1}; \quad (41)$$

$$(42)$$

At the real axis of τ the variables $\eta(\tau), \tilde{\eta}(\tau)$ will be complex conjugates, and the boundary value

$$f(\tau) = F_+(\eta(\tau)); \quad \forall \text{Im } \tau = 0 \quad (43)$$

Now we have an obvious analytic continuation to the lower semiplane of τ .

After some algebra we get⁷

$$\eta(\tau) = e^{t\beta/2} (1 + i\tau) \tau^{2k+1}; \quad (44)$$

$$f(\tau) = -i e^{-i\beta/2} \frac{\tau^{2k+1}}{2(4k+3)} \\ \left(c((8k+7)\tau + 8k+5) + e^{t\beta}(4k+3)(\tau - i)(2a+c) \right) \quad (45)$$

This parametric function in the sector $-\frac{\pi}{(k+1)} < \arg \tau < 0$ of the complex τ plane represents an implicit solution of the CVS equation.

Now, let us consider the limit $\tau \rightarrow \infty$ corresponding to $\eta \rightarrow \infty$. In this limit, the function $F_+(\eta(\tau))$ linearly grows

$$F_+(\eta) \rightarrow B\eta; \quad (46)$$

$$B = -a - \frac{1}{2}c \left(1 + \frac{e^{-i\beta}(8k+7)}{4k+3} \right) \quad (47)$$

This means that the true value of the xy components of strain at infinity is not $\text{diag}(a, -c - a)$ we thought it was. It is instead

$$\hat{S} = \begin{pmatrix} -\frac{c((8k+7)\cos(\beta)+4k+3)}{8k+6} & -\frac{c(8k+7)\sin(\beta)}{8k+6} \\ -\frac{c(8k+7)\sin(\beta)}{8k+6} & \frac{c(8k+7)\cos(\beta)-c(4k+3)}{8k+6} \end{pmatrix} \quad (48)$$

The eigenvalues of this strain are

$$\left\{ -\frac{c(6k+5)}{4k+3}, \frac{2c(k+1)}{4k+3} \right\} \quad (49)$$

Note that the angle β dropped from the eigenvalues. This happened because this angle can be eliminated by the $U(1)$ transformation $\eta \rightarrow \eta e^{-i\beta/2}$, which leaves the eigenvalues invariant.

The parabolic solution does not decrease at infinity, so it is inadequate for the turbulent statistics we develop later in this paper.

2.4. Hyperbolic curves

Let us now consider the hyperbolic curves with negative $\alpha < -\frac{1}{2}$, which do not need to be half integer. We redefine our parameters as follows:

$$\eta(\xi) = \pm e^{t\beta/2} (\xi + i\xi^{-\mu}); \quad (50)$$

$$\xi = \tau^{\alpha-\frac{1}{2}}; \quad (51)$$

$$\mu = \frac{1+2\alpha}{1-2\alpha}; \mu > 0; \quad (52)$$

$$0 < \xi < \infty \quad (53)$$

The two curves on Fig. 5, 6 correspond to various μ, β . Note that there are no singularities at the origin, as both curves are going around it.

There is a singularity of the inverse function at the point in the upper semiplane: where $\eta'(\xi_0) = 0$:

$$\xi_0 = (i\mu)^{\frac{1}{\mu+1}} \quad (54)$$

Therefore, we need to use the lower semiplane as a physical domain for $f(\xi) = F_+(\eta(\xi))$.

The holomorphic function $f(\xi)$ is reconstructed by means of the same steps as in the parabolic case. We get

$$f(\xi) = \frac{1}{2} e^{-\frac{1}{2}(i\beta)\xi} \xi \left(\frac{c(\mu-3)}{\mu-1} - e^{i\beta}(2a+c) \right) - \frac{ie^{-\frac{1}{2}(i\beta)\xi} \xi^{-\mu} \left(c(3\mu-1) + e^{i\beta}(\mu-1)(2a+c) \right)}{2(\mu-1)} \quad (55)$$

Let us now find the limit at $\xi \rightarrow \infty$, when η and f both linearly grow

$$f \rightarrow \eta B; \quad (56)$$

$$B = -a + \frac{1}{2}c \left(-1 + \frac{e^{-i\beta}(\mu-3)}{\mu-1} \right) \quad (57)$$

We would like this coefficient to be zero so that $f(\eta)$ decreases at infinity.

The solution of this complex equation for β, μ is

$$\begin{cases} \beta = 0; & \mu = 1 - \frac{c}{a}; \\ \beta = \pi; & \mu = 1 - \frac{c}{b}; \end{cases} \quad (58)$$

From the inequalities between the three eigenvalues $a < b < c$ adding to zero, we get

$$-2c < a < -\frac{c}{2}; \quad (59)$$

$$-\frac{c}{2} < b < c; \quad (60)$$

which makes this index μ limited to the interval

$$\begin{cases} \beta = 0; & \frac{3}{2} < \mu < 3; \\ \beta = \pi; & -\infty < \mu < \infty; \end{cases} \quad (61)$$

We choose the first solution, as in this case, μ varies in the positive region where there are no singularities.

Now, we observe that at $\beta = 0, \pi$, which means $q = 0$ there is an extra symmetry in the equation (25)

$$C \Rightarrow C^* \quad (62)$$

This means that now all four branches of the hyperbola

$$|y||x|^\mu = \text{const}; \quad (63)$$

are the parts of a single periodic solution $C(\theta)$ (Fig 7).

These four branches define the domain inside the loop C where the holomorphic velocity

$$F_-(\eta) = -2a\eta; \quad (64)$$

As for the function F_+ it is just a negative power

$$F_+(x \pm i|x|^{-\mu}) = +2ic|x|^{-\mu}; \quad (65)$$

The loop $C(\theta)$ defined by these four branches is a periodic function, with singularities at $\theta = k\pi/2$.

Topologically, on a Riemann sphere, these four branches divide the sphere into five regions. There is an inside region, with the boundary touching Riemann infinity four times.

Each of the four remaining outside regions is bounded by hyperbola, starting and ending at infinity. (Fig. 8).

Let us consider the lower right hyperbola with $y = -x^{-\mu}, x > 0$

The values of $F_+(\eta)$ in three other external regions will be obtained from this one by reflection against x or y axis.

$$F_+(-\eta) = -F_+(\eta); \quad (66)$$

$$F_+(\eta^*) = F_+^*(\eta); \quad (67)$$

We can continue the above parametric equation for the function f to the complex plane for the variable w , with the cut from $-\infty$ to 0. The phase of the multivalued function $w^{-\mu}$ is set to $\arg w^{-\mu} = 0, w > 0$.

$$\eta = w - iw^{-\mu}; \quad (68)$$

$$F_+ = 2icw^{-\mu}; \quad (69)$$

This parametric function has a square root singularity at the point where derivative $\partial_w \eta = 1 + i\mu w^{-\mu-1}$ vanishes:

$$w_c = (-i\mu)^{\frac{1}{\mu+1}} \quad (70)$$

For positive μ , this singularity is located in the lower semiplane of w , leaving the upper semiplane as a physical domain.

We have drawn the complex maps of the derivative $\partial_w \eta = 1 + i\mu w^{-\mu-1}$ for $\mu = 1.51, 2, 2.99$ (Fig. 9,10,11). We indicate the zeros of $\partial_w \eta$ as holes on the surface (white circles).

To check whether these singularities penetrate the physical region, we have drawn in black the boundaries of the physical regions

$$\mathbf{Re} \eta^\mu \mathbf{Im} \eta = \pm 1 \quad (71)$$

We observe that these square root singularities lie outside the physical region. This physical region is above the black line in the first quadrant, and there are no singular points there.

Inside the tube, the velocity is linear, and an extra linear term $F_-(\eta) = -2a\eta$; is potential, so that the incompressibility is preserved

$$V^- = ax - by - 2a(x + iy) = -ax + i(c - a)y \quad (72)$$

We show in Fig. 12 the streamline plot of this flow in the xy plane. We performed analytical and numerical computations in.⁸

While computing the complex velocity and coordinates using parametric equations, we restricted w to the physical region and populated this region by an irregular grid in angular variables in the w plane.

After that we used *ListStreamPlot* method of *Mathematica*[®].

The grid resolution does not allow tracking the boundary's immediate vicinity, but we computed the normal velocity numerically at the boundary. It turned out less than 10^{-15} on both sides of the sheet.

3. Viscous cutoff

The curve has an infinite length, and it encircles an infinite area because of the infinite cusps at $x = \pm 0, y = \pm 0$ (see Fig.7).

At a large upper limit $x_{max} \rightarrow \infty$ and small lower limit $x_{min} \rightarrow 0$ the perimeter of the loop goes as

$$P = 4R_0 \int_{x_{min}}^{x_{max}} dx \sqrt{1 + \mu^2 x^{-2(\mu+1)}} \rightarrow 4 \left(x_{min}^{-\mu} + x_{max} \right) R_0; \quad (73)$$

In the viscous fluid, with finite ν these infinities will not occur, of course. Our solution applies only as long as the spacing between the two branches of the hyperbola at Fig.7 is much larger than the viscous thickness of the vortex sheet.

$$h = \sqrt{\frac{\nu}{c}}; \quad (74)$$

$$x_{min} = \frac{h}{R_0}; \quad (75)$$

$$x_{max} = \left(\frac{R_0}{h} \right)^{\frac{1}{\mu}}; \quad (76)$$

$$P \rightarrow 4R_0 \left(\frac{R_0}{h} \right)^{\mu} + 4R_0 \left(\frac{R_0}{h} \right)^{\frac{1}{\mu}} \rightarrow 4R_0^{\mu+1} h^{-\mu} \quad (77)$$

To keep the perimeter fixed in the extreme turbulent limit, we have to tend the parameter R_0 to zero as

$$R_0 = \left(\frac{P}{4} \right)^{\frac{1}{\mu+1}} \left(\frac{\nu}{c} \right)^{\frac{\mu}{2(\mu+1)}} \rightarrow 0; \quad (78)$$

4. Velocity Gap and Circulation

Once the equation is solved, the parametric solution for Γ is straightforward (with factors of R_0 restored from dimensional counting)

$$\Gamma = \int (-2aXX' + 2(a-c)YY')dx = -aR_0^2 \left(x^2 - \mu|x|^{-2\mu} \right); \quad (79)$$

$$\Delta V = \frac{\Gamma'}{C'} = -2aR_0x \left(1 + \mu|x|^{-\mu-1} \right) \quad (80)$$

We have not expected to find such a singular vortex tube, but it satisfies all requirements and must be accepted.

In,⁵ we appealed to the Brouwer theorem⁹ to advocate the existence of solutions of the CVS equations. This theorem does not tell us how many fixed points are on a sphere made of the normalized Fourier coefficients in the limit their number going to infinity. Perhaps, there are also some nonsingular solutions.

This singular solution is not normalizable, and it has a vanishing circulation

$$\Delta\Gamma = \frac{cR_0^2}{\mu-1} \left(x^2 - \mu|x|^{-2\mu} \right)_{x=-\infty}^{x=\infty} = 0 \quad (81)$$

Thus, the Brouwer theorem does not apply here – this is a more general case than the one assumed in.⁵ On the other hand, we do not need an existence theorem anymore once we have found an analytic solution.

Note that the net circulation would be infinite unless we combine all four branches of our hyperbola into a single closed-loop (with cusps at the real and imaginary axes, but still closed).

5. Minimizing Euler Energy

Let us now compute the energy of the vortex surface as a Hamiltonian system.^{10, 11} There is a regular part related to the background strain. This part is not involved in the minimization we are interested in; it depends on a, b, c , which are external parameters for our problem.

The internal part of the Hamiltonian is directly related to the potential gap Γ we have computed in the previous section.

$$H_{int} = \int_{\vec{r}_1, \vec{r}_2 \in \mathcal{S}} d\Gamma(\vec{r}_1) \wedge d\vec{r}_1 \cdot d\Gamma(\vec{r}_2) \wedge d\vec{r}_2 \frac{1}{8\pi|\vec{r}_1 - \vec{r}_2|} \quad (82)$$

In our case of cylindrical surface

$$d\Gamma(\vec{r}_1) \wedge d\vec{r}_1 = d\Gamma(\theta) \{0, 0, dz\} \quad (83)$$

and we have a separation of variables θ, z .

The integration over z_1, z_2 provides the total length $L \rightarrow \infty$ of the cylinder times logarithmically divergent integral over $z_1 - z_2$. We limit this integral to the

interval $(-L, L)$ and compute it exactly

$$\int_{-L}^L \frac{1}{8\pi\sqrt{\eta^2 + z^2}} dz = \frac{\log\left(\frac{2L(\sqrt{\eta^2 + L^2} + L)}{\eta^2} + 1\right)}{8\pi} \quad (84)$$

Then we expand it for large L

$$\int_{-L}^L \frac{1}{8\pi\sqrt{\eta^2 + z^2}} dz \rightarrow \frac{\log(2L) - \log|\eta|}{4\pi} + O\left(\frac{\eta^2}{L^2}\right) \quad (85)$$

Thus we get in our case, with $\Gamma'(w)$ from (79)

$$\frac{H_{int}}{L} = \log(2L) \frac{(\Delta\Gamma)^2}{4\pi} - \frac{1}{8\pi} \int_{-\infty}^{\infty} dw_1 \Gamma'(w_1) \int_{-\infty}^{\infty} dw_2 \Gamma'(w_2) \log|\zeta_1 - \zeta_2|; \quad (86)$$

$$\zeta_{1,2} = w_{1,2} - \iota |w_{1,2}|^{-\mu}; \quad (87)$$

$$\Gamma'(w) = \frac{2cR_0^2 w}{\mu - 1} \left(1 + \mu^2 |w|^{-2\mu-2}\right) \quad (88)$$

At $L \rightarrow \infty$ the first term is the leading one. Minimization of the energy leads to the condition

$$\Delta\Gamma = 0 \quad (89)$$

Therefore, our solution with zero circulation is singled out among other combinations of hyperbolic vortex sheets by the requirement of minimization of energy.

Once the divergent term vanishes, one can compute the rest of the energy.

The remaining principal value integral over x_1, x_2 converges at infinity. In the local limit, when $R_0 \rightarrow 0$, it goes to zero.

We do not see a point in this computation compared to observable quantities such as the energy dissipation and the Wilson loop.

6. The induced background strain

What is the physical origin of the constant background strain $W_{\alpha\beta}$ which we used in our solution?

Traditionally, the ad hoc Gaussian random forces are added to the Navier-Stokes equation to simulate the effects of the unknown inner randomness.

We do not think that this beautiful equation needs any crutches; it can walk all by itself.

In our theory, the random forces come from many remote vortex structures, contributing to the background velocity field via the Biot-Savart law.

These forces are not arbitrary; they are rather self-consistent, like a mean field in ordinary statistical mechanics.

Let us assume that the space is occupied by some localized CVS structures far from each other. In other words, let us consider an ideal gas of vortex bubbles.

This ideal gas approximation is close to reality, where the vorticity occupies a small subset of the physical space with fractal dimension^{10,11} $D_f \approx \frac{7}{3} < 3$.

We shall see below that the mean size R_0 of the surface is small compared to the mean distance \bar{R} between them in the turbulent limit $\nu \rightarrow 0, \mathcal{E} = \text{const}$. This vanishing size vindicates the assumptions of the low-density ideal gas.

In such an ideal gas, we can neglect the collision of these extended particles, but not the long-range effect of the strain they impose on each other.

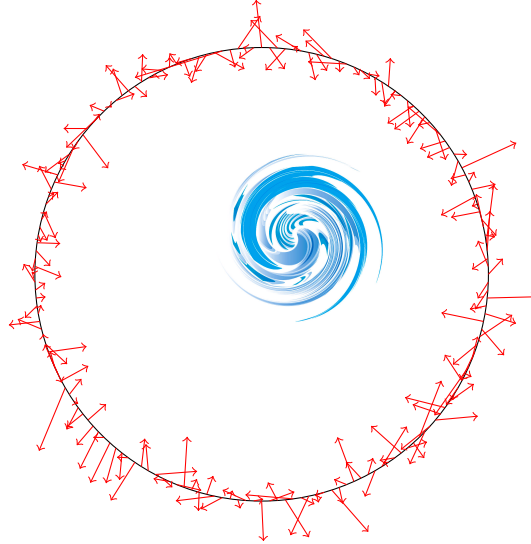
The Biot-Savart formula for the velocity field induced by the set of remote localized vorticity bubbles B

$$\vec{v}(\vec{r}) = \sum_B \int_B d^3r' \frac{\vec{\omega}(\vec{r}') \times (\vec{r}' - \vec{r})}{4\pi|\vec{r}' - \vec{r}|^3} \quad (90)$$

falls off as $1/r^2$ for each bubble, like an electric field from the charged body.

Note that all vortex structures in the volume contribute to this background velocity field, adding up to a large number of small terms at every point in space.

If there are many such bubbles distributed in space with small but finite density, we would have the "night sky paradox." The bubbles spread on the far away sphere will compensate the inverse distance squared for a divergent distribution like $\int R^2 dR/R^2$.



This estimate is, of course, wrong, as the velocity contributions from various bubbles are uncorrelated, so there is no coherent mean velocity.

Moreover, a Galilean transformation would remove the finite background velocity, so it does not have any physical effects.

However, with the strain, there is another story. Strain coming from remote

vortex bubbles

$$W_{\alpha\beta}(\vec{r}) = e_{\alpha\mu\gamma} \partial_\beta \partial_\gamma \sum_B \int_B d^3 r' \frac{\omega_\mu(\vec{r}')}{4\pi |\vec{r} - \vec{r}'|} \quad (91)$$

falls off as $1/r^3$, and this time, there could be a mean value \bar{W} , coming from a large number of random terms from various bubbles with distribution $R^2 dR/R^3 \sim dR/R$.

The space symmetry arguments and some refined arguments we present in the next section tell us that averaging over the directions of the bubble centers $\vec{R} = \vec{r}' - \vec{r}$ completely cancels this mean value.

The Central Limit Theorem suggests (within our ideal vortex gas model) that such a strain would be a Gaussian tensor variable, satisfying the normal distribution of a symmetric traceless matrix with zero mean

$$dP_\sigma(W) \propto \prod_i dW_{ii} \prod_{i<j} dW_{ij} \delta\left(\sum_i W_{ii}\right) \exp\left(-\frac{\text{tr } W^2}{2\sigma^2}\right) \quad (92)$$

This distribution was studied extensively in physics and mathematics, so we are not giving references here. Separating SO_3 rotations $\Omega \in S_2$, we have the measure for eigenvalues a, b, c :

$$dP_\sigma(W) = \frac{1}{4\pi} d\Omega da db dc \delta(a+b+c) P_\sigma(a, b, c); \quad (93)$$

$$P_\sigma(a, b, c) = \sqrt{\frac{3}{\pi}} \theta(b-a) \theta(c-b) (b-a)(c-a)(c-b) \exp\left(-\frac{a^2 + b^2 + c^2}{2\sigma^2}\right) \quad (94)$$

7. Energy dissipation and its distribution

The general formula⁵ for the surface dissipation reads

$$\mathcal{E} = \frac{\sqrt{\nu}}{2\sqrt{\pi}} \int_D d^2 \xi \sqrt{g} \sqrt{-S_{nn}} (\Delta \vec{v})^2; \quad (95)$$

As we noticed in the previous work⁵ this surface dissipation is conserved on CVS surfaces.

Without CVS as a stability condition, the dissipation itself would not be an integral of motion, undermining the hypothesis of the steady energy flow, which is central to any modern theory or model of turbulence.

For our hyperbolic loop solution the energy dissipation integral reduces to the following expression (where we restore the implied spatial scale R_0 and expressed the cutoffs in terms of the perimeter P of the loop by (78))

$$\frac{\mathcal{E}}{L\sqrt{\nu}} = 4 \frac{2a^2\sqrt{c}}{\sqrt{\pi}} R_0^3 \int_{x_{min}}^{x_{max}} dw w^2 \left| 1 - \mu w^{-\mu-1} \right|^3 \rightarrow P^3 \frac{a^2\sqrt{c}}{24\sqrt{\pi}} \quad (96)$$

The normalized distribution $W(\zeta)$ for the scaling variable ζ takes the form¹²

$$W(\zeta) = 2\zeta^{9/5} \sqrt{\frac{3}{\pi}} \int_{2^{-1/5}}^{2^{1/5}} dy \frac{(2-y^5)(y^5+1)(2y^5-1)}{y^{14}} \exp\left(\frac{(-y^{10}+y^5-1)\zeta^{4/5}}{y^8}\right) \quad (97)$$

$$\zeta = \frac{24\sqrt{\pi}\mathcal{E}}{LP^3\sqrt{\nu\sigma^5}}; \quad (98)$$

The expectation value of this scaling variable equals to

$$\bar{\zeta} = 4.90394 \quad (99)$$

We show at Fig.13 the log-log plot of this distribution.

This $W(\eta)$ is a completely universal function. We would verify this prediction when the distribution of energy dissipation in numerical or real experiments in the extreme turbulent regime will become available.

8. Dilute gas of vortex bubbles in mean-field approximation

Let us elaborate on this idea of a dilute gas of vortex bubbles and compute the strain variance.

Consider a large number of independent vortex bubbles, sparsely distributed in the 3D volume.

The net strain near this surface will come from the Biot-Savart formula, which we expand at large distances (plus symmetric terms with swapped α, β)

$$W_{\alpha\beta}(\vec{r}) \rightarrow e_{\alpha\mu\gamma} \left(\Omega_\mu \partial_\beta \partial_\gamma + \Omega_{\mu\lambda} \partial_\beta \partial_\gamma \partial_\lambda + \dots \right) \frac{1}{4\pi|\vec{r}|}; \quad (100)$$

$$\Omega_\mu = \int_B d^3 r' \omega_\mu(\vec{r}'); \quad (101)$$

$$\Omega_{\mu\lambda} = \int_B d^3 r' \omega_\mu(\vec{r}') r'_\lambda \quad (102)$$

The comment is in order. At zero viscosity, the surface is infinite, and the integrals for multipole moments $\Omega_{\mu\dots}$ diverge.

We consider the case of small but finite viscosity when the surface is finite due to the viscous cutoff at the cusps. We assume the distance r to be much larger than the size of this clipped surface. This assumption will be vindicated below.

The contribution to the strain from each remote vortex blob will be linearly related to these multipole moments of vorticity.

These vectors and tensors are random variables with zero mean^a, in addition to the random locations on a sphere, which is why we expect the Central Limit Theorem to apply here).

The vorticity for each vortex bubble S is given by a surface integral^{10,11}

$$\omega_v(\vec{r}) = \int_S d\Gamma \wedge dr'_v \delta^3(\vec{r} - \vec{r}'); \quad (103)$$

$$\Omega_\mu = \int_S d\Gamma \wedge dr_\mu; \quad (104)$$

$$\Omega_{\mu\lambda} = \int_S d\Gamma \wedge dr_\mu r_\lambda \quad (105)$$

We get exactly zero when averaged over directions of the position vector \vec{r} of the bubble on the large sphere. We verified that up to the fourth term by symbolic integration.¹³ There is, of course, a general reason for these cancellations.

The rotational average of the multiple derivative matrix has only one totally symmetric symmetric tensor structure

$$\begin{aligned} T_{\mu_1 \dots \mu_n} &= \left\langle \partial_{\mu_1} \dots \partial_{\mu_n} \frac{1}{|\vec{r}|} \right\rangle_{\vec{r} \in S_2} = \\ &= C \left(\delta_{\mu_1 \mu_2} \dots \delta_{\mu_{n-1} \mu_n} + \text{permutations} \right) \end{aligned} \quad (106)$$

However, the contraction over any pair of indices yields zeroes because $\frac{1}{|\vec{r}|}$ satisfies the Laplace equation. Therefore $C = 0$.

The number dN of the vortex structures on the large sphere would be estimated as

$$dN = 4\pi\rho(R)R^2 dR \quad (107)$$

where $\rho(R)$ is the distribution of distances between the vortex structures.

After some tensor algebra and symbolic angular integration¹³ we found the formula for σ with separated averaging over the unit vector on a sphere S_2 and the random tensor W

$$5\sigma^2 = \frac{9}{2\pi^2} \langle \Omega_{\alpha\beta}^2 \rangle_W 4\pi \int dR \frac{\rho(R)}{R^6}; \quad (108)$$

This distribution is normalized as

$$4\pi \int dR \rho(R) R^2 = 1 \quad (109)$$

^aThe directions of these vectors in our exact solution coincide with one of the eigenvectors of the local strain tensor at the location of that particular CVS surface. Assuming random locations in space, so will be the strain tensors and so will be the vorticity vectors (directed along the symmetry axis of the cylindrical solution).

Therefore, our expression involves a mean value of $1/R^8$

$$\left\langle \frac{1}{R^8} \right\rangle = \frac{\int dR \rho(R) R^{-6}}{\int dR \rho(R) R^2}; \quad (110)$$

$$\int dR \rho(R) R^{-6} = \frac{1}{4\pi} \left\langle \frac{1}{R^8} \right\rangle \quad (111)$$

After that, we relate the variance to the mean squared vorticity of each vortex structure and the relative distance distribution of these tubes.

$$\sigma^2 = \frac{9}{10\pi^2} \left\langle \Omega_{\alpha\beta}^2 \right\rangle_W \left\langle \frac{1}{R^8} \right\rangle \quad (112)$$

In our theory, with a cylindrical tube of size L

$$\Omega_{\alpha\beta} = L \left(\delta_{\alpha z} I_\beta - \delta_{\beta z} I_\alpha \right); \quad (113)$$

$$I_z = 0; \quad (114)$$

$$I_x + i I_y = \oint_C d\Gamma C = \frac{2cR_0^3}{3(\mu-1)} \left[x^3 + \frac{3\mu^2 x^{1-2\mu}}{1-2\mu} - \frac{3i|x|^{2-\mu}}{\mu-2} - i\mu|x|^{-3\mu} \right]_{x=-x_{max}}^{x=x_{max}} \quad (115)$$

In the turbulent limit $x_{max} \rightarrow \frac{P}{4R_0}$ we find

$$I_x + i I_y \rightarrow \frac{cP^3}{48(\mu-1)} \quad (116)$$

After integrating over the eigenvalues a, b, c , we find the following expression for the variance of strain

$$\sigma^2 = \sigma^2 \frac{L^2}{3(16\pi)^2} \left\langle P^6 \right\rangle \left\langle \frac{1}{R^8} \right\rangle; \quad (117)$$

$$\bar{R} = \left\langle \frac{1}{R^8} \right\rangle^{-\frac{1}{8}} \quad (118)$$

The variance cancels here and this brings us to the final result for the mean energy dissipation

$$\langle \mathcal{E} \rangle \propto \bar{L} P^3 \sqrt{\nu \sigma^5}; \quad (119)$$

$$L^2 \left\langle P^6 \right\rangle = 3(16\pi)^2 \bar{R}^8; \quad (120)$$

Let us be specific about the geometry scale here: we choose the mean distance between vortex structures \bar{R} as a universal length scale. The sizes of the individual CVS surfaces vary and fluctuate, but this \bar{R} is a global parameter of our system so that we can use it as a unit of length.

The energy dissipation (for a single CVS surface) in this case scales as

$$\langle \mathcal{E} \rangle \propto \bar{R}^4 \sqrt{\nu \sigma^5}; \quad (121)$$

$$(122)$$

Thus, we get a scaling relation in the turbulent limit, the same we assumed in previous papers^{5,14}

$$\sigma \sim \left(\frac{\mathcal{E}}{\bar{R}^4} \right)^{\frac{2}{5}} \nu^{-\frac{1}{5}} \quad (123)$$

The mean perimeter P of the CVS tube, when measured in these units shrinks with the length L of this tube as

$$\frac{P}{\bar{R}} \sim \left(\frac{\bar{R}}{L} \right)^{\frac{1}{3}} \quad (124)$$

The radius of the tube, in this case, shrinks with an extra positive power of viscosity

$$\frac{R_0}{\bar{R}} \propto \left(\frac{\bar{R}}{L} \right)^{\frac{1}{3}} \left(\frac{\nu}{\sigma} \right)^{\frac{\mu}{2(\mu+1)}} \propto L^{-\frac{1}{3}} \nu^{\frac{3\mu}{5(\mu+1)}} \quad (125)$$

The last two estimates vindicate the assumption of the dilute gas approximation: the mean perimeter P of our vortex particles is much smaller than their mean separation \bar{R} . At the same time, the multipole expansion is justified, as the distance \bar{R} is larger than the finite size of each vortex surface.

The mean extent $\langle |\Delta r| \rangle$ of the surface which we estimate in the next section, scales in the turbulent limit as

$$\left\langle \frac{|\Delta r|}{\bar{R}} \right\rangle \sim \left(\frac{\bar{R}}{L} \right)^{\frac{1}{3}} \nu^{-\frac{3}{5(\mu+1)}} \quad (126)$$

The first factor is small at large L ; the second one grows with vanishing viscosity.

As we do not yet know the mechanism leading to the termination of the cylindrical tube, the estimate of L in the turbulent limit remains an open problem.

At least, we may assume that $L \gg \langle |\Delta r| \rangle$. It would be sufficient for the justification of the dilute gas approximation.

9. "Multi-fractals"

Our hyperbolic vortex tube $|y||x|^\mu = \text{const}$ is smooth, but its shape has a random power index μ . The fluctuating power indexes imitate the multifractal scaling laws without any conventional fractals present.

Let us start with relation between the mean distance Δr between two points and the perimeter P of our curve. Both variables tend to infinity in a turbulent

limit, but there is an asymptotic power law

$$P = 4 \int_{x_{min}}^{x_{max}} dw |C'(w)| \propto R_0 x_{min}^{1-\mu}; \quad (127)$$

$$C' = \left| 1 + i \mu w^{-\mu-1} \right|; \quad (128)$$

$$\begin{aligned} \langle |\Delta r| \rangle &= 4 \iint_{x_{min}}^{x_{max}} dw_1 dw_2 |C'(w_1)| |C'(w_2)| \\ &\frac{|C_1 - C_2| + |C_1 - C_2^*| + |C_1 + C_2| + |C_1 + C_2^*|}{P^2} \propto R_0 x_{min}^{-\mu}; \end{aligned} \quad (129)$$

If we take this as an ordinary relation between the volume and size of d -dimensional manifold, we would have to assign to this curve the fractal dimension

$$d = \frac{d \log P}{d \log |\Delta r|} = \frac{\mu - 1}{\mu} \quad (130)$$

This dimension is not a constant. As it follows from the random matrix distribution, this dimension is a random variable distributed between $1/3$ and $2/3$ with the normalized density¹²

$$W(d) = \frac{3\sqrt{3}(2-3d)(3d-1)}{8(3d^2-3d+1)^{5/2}} \quad (131)$$

We plotted this distribution at Fig. 14.

It is fluctuating below 1, which is interesting by itself. The typical fractal curves like a Brownian path have a fractal dimension above 1.

The reason is that our curve is smooth, and it has a very special infinite shape, which makes its average point difference grow faster than its length.

One could argue that this does not fit some other definition of a fractal, but this is beside the point: various functionals on our curve fluctuate as if the curve has a fractal dimension fluctuating between $1/3$ and $2/3$, whether we call it a fractal or not.

Let us now turn our attention to the most interesting functional, the velocity difference, related to the velocity gap in our theory.

Velocity field in the CVS theory is potential everywhere in space, except the thin layers surrounding our hyperbolic vortex sheets.

The velocity difference between two neighboring points \vec{r}_1, \vec{r}_2 in the potential flow with scale as $\vec{r}_1 - \vec{r}_2$ as the harmonic potential has no singularity.

However, with some probability, these two points will be separated by a vortex surface, in which case there will be a finite gap $\Delta \vec{v}$.

The estimate of the velocity difference moments would involve integration over the translation, rotation, and eigenvalues of the strain tensor.

Schematically, assuming $\vec{r}_1 = (x_1, y_1, z)$ outside our vortex tube, and $\vec{r}_2 = (x_2, y_2, z)$ inside, we have (with \hat{r} being unit vector of $\Delta \vec{r}$, $\eta_1 = x_1 + i y_1, \eta_2 =$

$x_2 + iy_2$):

$$\langle (\Delta \vec{v} \cdot \hat{r})^n \rangle \sim \int dP_\sigma(W) \int_{\Sigma(\Omega)} dx_1 dy_1 dx_2 dy_2 \left(\text{Re} \left(ax_1 - iy_1 + F_+(\eta_1) + ax_2 + (a-c)iy_2 \right) \frac{\eta_2^* - \eta_1^*}{|\eta_2 - \eta_1|} \right)^n; \quad (132)$$

$$\Sigma(\Omega) : |y_{1,2}| |x_{1,2}|^\mu > 1, \Omega \cdot (\vec{r}_2 - \vec{r}_1) = (|\Delta \vec{r}|, 0, 0); \quad (133)$$

$$\eta_1 = x_1 + iy_1, \eta_2 = x_2 + iy_2; \quad (134)$$

The measure for the traceless random 3×3 matrices $dP_\sigma(W)$ is presented in (93). The nontrivial part is the $SO(3)$ integration measure over the 3D rotations Ω involved in that measure. The distribution of the ratio of eigenvalues a, b, c in (93) leads to the distribution of the index $\mu = 1 - \frac{c}{a}$.

Integrating over the highest eigenvalue c at fixed μ and scaling $|\Delta r|$ out of all coordinates we get:¹²

$$\langle (\Delta \vec{v} \cdot \hat{r})^n \rangle \sim \int d\Omega \int_{\Sigma(\Omega)} dx_1 dy_1 dx_2 dy_2 \int_{\frac{3}{2}}^3 d\mu Q_n(\mu) |\Delta r|^{n+4} \left(\text{Im} \left(\frac{2}{|\Delta r| w_1 (\eta_1)^\mu} + \frac{\mu(y_1 - y_2) + i(x_1 + x_2 + 2iy_1)}{\mu - 1} \right) \frac{\eta_2^* - \eta_1^*}{|\eta_2 - \eta_1|} \right)^n; \quad (135)$$

$$\Sigma(\Omega) : |\Delta r|^{\mu+1} |y_{1,2}| |x_{1,2}|^\mu > 1, \Omega \cdot (\vec{r}_2 - \vec{r}_1) = (1, 0, 0); \quad (136)$$

$$Q_n(\mu) = \frac{\sqrt{3} \Gamma\left(\frac{n+5}{2}\right) (3-\mu)\mu(2\mu-3)(\mu-1)^n}{2\sqrt{\pi}((\mu-3)\mu+3)^{\frac{1}{2}(n+5)}}; \quad (137)$$

$$|\Delta r| \eta_1 = x_1 + iy_1, |\Delta r| \eta_2 = x_2 + iy_2; \quad (138)$$

$$|\Delta r| \eta_1 = w_1 - iw_1^{-\mu} \quad (139)$$

In this integral, the pair of points $(x_1, y_1), (x_2, y_2)$ are sliding along the curve while staying on different sides, separated by a fixed distance 1. The dependence upon $|\Delta r|$ is manifest now.

We do not expect this dependence to result in exact form $\langle (\Delta \vec{v} \cdot \hat{r})^n \rangle \propto |\Delta \vec{r}|^{\zeta(n)}$ assumed in the multifractal scaling law. It is a more complicated function of two variables $n, \log |\Delta \vec{r}|$. The saddle point approximation of this integral could imitate a multifractal scaling law.

Our vortex sheet solution explicitly breaks the time-reversal symmetry; therefore, the odd moments do not vanish. The interchange of the two coordinates $\vec{r}_2 \leftrightarrow \vec{r}_1$ changes the velocity field significantly.

There is a way to estimate the multifractal scaling law from our theory without computing this multidimensional integral (which we plan to do eventually).

In a recent work of Sreenivasan and Yakhot¹⁵ it was argued that with the

"renormalized" Bernoulli formula for the pressure

$$p = -\frac{1}{2}\alpha\bar{v}^2; \quad (140)$$

$$\alpha \approx 0.95 \quad (141)$$

the Hopf chain of equations for the velocity moments $\langle |\Delta v(\vec{r})|^n \rangle$ can be closed, providing relations for the multi-fractal exponents, closely matching those observed in numerical simulations.

As we know that the Bernoulli equation is not valid in a turbulent flow, this observation looks like a paradox.

However, in the CVS theory, these estimates make sense.

For the (majority of) points in space outside the vortex surface, the original Bernoulli formula, with $\alpha = 1$, holds. We reinterpret coefficient α as a probability of having no vorticity in a given point, involved in the computation of the Hopf moments.

The unconditional probability of avoiding a randomly translated and rotated smooth surface at a given point in space equals 1. However, there are several reasons for this probability α to be less than 1.

One is the finite thickness of the vortex sheet:

$$h \propto \sqrt{\frac{v}{\sigma}} \sim v^{\frac{3}{5}} \sim \text{Re}^{-\frac{1}{2}} \quad (142)$$

With $\text{Re} \sim 10^4$, this thickness measures in percents of the mean radius, which by itself can explain the 5% deviation from 1.

Another reason is that in the conditions used to compute the Hopf equations for the velocity moments, a vortex surface must be present between the two points \vec{r}_1, \vec{r}_2 . However, each of these two points belongs to the potential flow region.

The conditional probability of having a vortex sheet between two points would be finite, providing another source of renormalization of the Bernoulli law.

The arguments involved in¹⁵ were relying on the turbulent viscosity notion, which we do not know how to justify in our theory. Still, the turbulent viscosity is an existing effect in the complementary approach with fluctuating velocity field. Perhaps, our effect of avoiding the vortex sheet is a dual description of the same phenomenon of turbulent viscosity.

The complete theory would have to compute the moments from the first principle. Then we will find the full function of two variables $n, \log |\Delta r|$, currently approximated by the multifractal scaling law.

10. Wilson Loop Statistics

Let us assume that we have some CVS surface parameterized by the random tensor $W = \text{diag}(a, b, c)$.

There are space translations, factored by a cylindrical translation in the z axis and parameters of the symmetric traceless matrix W : two eigenvalues $c > 0, a \in$

$(-2c, -c/2)$ plus arbitrary rotations $\Omega \in S_2$ of the coordinate system.

As we described in the previous sections, we treat this W as the background uniform strain created by other vortex structures far away from the surface's axis. Thus, one would think that this strain, adding up strains from a large number of randomly positioned vortex structures like this one, would be a random traceless symmetric tensor.

The z axis of the tube automatically aligns with the leading eigenvector of W , the one with the largest eigenvalue $c > 0$. The CVS stability requires this.

There remains an integral over zero modes: translation and rotation of the coordinate system plus two eigenvalues of the random constant strain at infinity. We should integrate over these parameters the observables computed for a particular solution of CVS.

To be specific, let us consider the loop average

$$W_C(\gamma) \propto \int d^3 r_0 d\Omega dP(p, q) \exp \left(i \gamma \oint_C v_\alpha(\vec{r}) dr_\alpha \right) \quad (143)$$

The velocity circulation in the exponential comes only from the intersection points of the loop C with our cylindrical surface. A simple loop intersects the surface in two points or does not intersect at all, so we have

$$\Gamma_{12} = \oint_C v_\alpha dr_\alpha = \Gamma(\eta_2) - \Gamma(\eta_1) \quad (144)$$

Thus, up to extra terms independent of γ

$$W_C(\gamma) \propto \int d^3 r_0 d\Omega dP(a, b) \Pi_S(\vec{r}_0, \Omega, \gamma) \quad (145)$$

The factor

$$\begin{aligned} \Pi_S(\vec{r}_0, \Omega, \gamma) &= \int_0^1 dl_1 |C'(l_1)| \int_0^1 dl_2 |C'(l_2)| \\ &\int_{\vec{r}_1 \in S} \int_{\vec{r}_2 \in S} \delta^3 \left(\vec{r}_1 + \Omega \cdot (\vec{r}_0 - \vec{C}(l_1)) \right) \delta^3 \left(\vec{r}_2 + \Omega \cdot (\vec{r}_0 - \vec{C}(l_2)) \right) \\ &\exp \left(i \gamma (\Gamma(\eta_2) - \Gamma(\eta_1)) \right) \end{aligned} \quad (146)$$

was already computed in¹⁶

$$\begin{aligned} \Pi_S(\vec{r}_0, \Omega, \gamma) &= \frac{|\vec{\sigma}_1| |C'(l_1)|}{\left| \vec{\sigma}_1 \cdot \Omega \cdot \vec{C}'(l_1) \right|} \frac{|\vec{\sigma}_2| |C'(l_2)|}{\left| \vec{\sigma}_2 \cdot \Omega \cdot \vec{C}'(l_2) \right|} \theta(\vec{r}_1 \in S) \theta(\vec{r}_2 \in S) \\ &\exp \left(i \gamma (\Gamma(\eta_2) - \Gamma(\eta_1)) \right); \end{aligned} \quad (147)$$

$$\vec{\sigma}_1 = \vec{\sigma}(\vec{r}_1); \vec{\sigma}_2 = \vec{\sigma}(\vec{r}_2); \quad (148)$$

$$\vec{r}_1 = \Omega \cdot (\vec{C}(l_1) - \vec{r}_0); \vec{r}_2 = \Omega \cdot (\vec{C}(l_2) - \vec{r}_0); \quad (149)$$

This integral depends on the geometry of the problem: the relation between the loop C and the cylinder. The phase factor depends on the random strain parameters via known $\Gamma(\eta)$.

We are left with an integral over $2d$ translations \vec{r}_0 against the cylinder's axis and the O_3 rotations Ω .

The two theta functions, restricting the points to be on the intersection of the surface and the loop, are zero if the point \vec{r}_0 moves from the surface farther than the maximal size of the loop C .

The integration region for \vec{r}_0 is some layer around the vortex surface, with the width equal to the maximal distance between two points on the loop.

The integration over rotations Ω is compact. Therefore, this integral looks like a relatively straightforward integral from a computational point of view.

As we already mentioned, there is no time-reversal symmetry that would reflect γ . Therefore, the flux $\Delta\Gamma$ is the same sign as q in our irreversible solution.

As a consequence, our Wilson loop will be a complex number. Unfortunately, nobody has measured it in DNS, but its Fourier transform (over circulation, not over space coordinates) represents the circulation PDF measured with high accuracy.

This Fourier transform would simply mean replacement

$$\exp(i\gamma(\Gamma(\eta_2) - \Gamma(\eta_1))) \Rightarrow \delta\left((\Gamma(\eta_2) - \Gamma(\eta_1)) - \oint_C \vec{v} \cdot d\vec{r}\right) \quad (150)$$

This delta function is welcome, as it will reduce the dimension of the remaining integration over \vec{r}_0 .

After that, *Mathematica*[®] can compute this finite integral with arbitrary precision.

Another possibility is to compute the moments of the circulation $M_n = \left\langle \left(\oint_C \vec{v} \cdot d\vec{r}\right)^n \right\rangle$ which would correspond to the replacement

$$\exp(i\gamma(\Gamma(\eta_2) - \Gamma(\eta_1))) \Rightarrow ((\Gamma(\eta_2) - \Gamma(\eta_1)))^n \quad (151)$$

Thus, there is a steep but clear path to compute a Wilson loop using the above formulas.

11. Discussion

The CVS theory offers an approach to turbulence that one can study analytically and numerically.

Let us remind and discuss the general ideas behind this theory.

We are trying to solve the Navier-Stokes equations for an infinite time evolution, given that the laminar flow is unstable. This unstable solution could cover the whole phase space of the fluid mechanics; however, we suspect that there are some low-dimensional attractors in that space.

The solution would cover the subspace of these attractors like the Newtonian dynamics covers the energy surface in ergodic motion.

We also know the phenomenon of anomalous dissipation: the dissipation in extreme turbulence occurs in the regions of high vorticity, which compensates for the viscosity factor in front of the enstrophy integral.

Furthermore, we conjecture that these regions of high vorticity are vortex surfaces. There are several reasons to believe so, both theoretical and (numerical or real) experimental sides.

The Hamiltonian dynamics of vortex surfaces^{10,11} can be solved exactly in some important cases, and the resulting solutions have all nice properties, including anomalous dissipation.

We have found in our previous work^{14,16} that the steady-state of the vortex surface is a promising candidate for such an attractor in phase space. At first sight, it appears that these steady vortex surfaces have some local degrees of freedom, corresponding to the arbitrary shape of the surface, as long as the velocity gap satisfies certain integral equations, following from the minimization of the Hamiltonian.

Initially, we speculated that these surface degrees of freedom were described by some version of a solvable string theory.¹⁶ There are two kinds of surface degrees of freedom: the surface shape and the internal metric on this surface, described by the Liouville field.

In fluid dynamics terms, the fluctuations of this internal metric correspond to the tangent motions of the fluid, equivalent to the re-parametrization of this surface.

The shape of the surface was assumed frozen in the turbulent flow in,¹⁶ and the remaining internal metric was assumed to be responsible for the multifractal scaling laws for the moments of velocity circulation.

The new recent understanding eliminated the shape of the surface as degrees of freedom while placing no restrictions on the internal metric on this surface.

Some surfaces are "more equal" than others because they are stable at the microscopic level. These are the CVS surfaces satisfying the stability equations (1).

It is truly remarkable that such a simple equation, involving just three letters, leads to so many specific consequences for the turbulent flow.

The negative normal strain presses vorticity into the CVS surface from both sides, leading to a narrow Gaussian profile of vorticity in the normal direction. The width of this boundary layer goes to zero as some negative power of Reynolds number in the turbulent limit.

We assume that our flow and the surface are subject to a background strain, a random traceless matrix adding up from Biot-Savart tails of many other vortex structures located far away from this one. Such random strain is described by eigenvalues a, b, c adding up to zero. The parameters a, b, c obey a Gaussian distribution multiplied by a famous Vandermonde determinant.

The normal strain is uniform all around our vortex surface $S_{nn} = -c$, so that we have one of the stability criteria fulfilled if the axis of the vortex tube points along the main eigenvector of the strain, with a positive eigenvalue c . The tangent strain is degenerate: there is zero strain along the tangent velocity gap.

The energy dissipation occurs at the surface, and we have demonstrated⁵ that

this surface integral is conserved in the Navier-Stokes dynamics in the turbulent limit.

Let us stop and think about this conservation law. It is *not* an Euler conservation law, violated by viscosity, like the energy conservation. Instead, we have found a previously unknown Navier-Stokes conservation law, and it comes about as a result of the exact cancellation of the vortex stretching and diffusion terms in the Navier-Stokes equation used for the time derivative of the enstrophy.

The Euler dynamics would lead to an explosion or decay of enstrophy were it not offset by the diffusion in full Navier-Stokes equation. For any other vortex surface but the CVS the diffusion would not cancel the vortex stretching so that the notorious energy dissipation constant \mathcal{E} would not be constant.

The Kolmogorov theory kept this skeleton in the closet for 80 years. The basic constant of the theory was time-dependent, after all. Better to say, it *was* constant with one definition (three-point function of velocity), but not with an alternative one (enstrophy), and nobody knew why.

As we see it now, \mathcal{E} is conserved because of the CVS stability of the vortex surfaces hidden behind the rough picture of the energy flow in Fourier space. One cannot describe the shape of the discontinuity surface by a finite (or even convergent) set of Fourier coefficients of the velocity field – it is like describing Mona Lisa's smile by the spectral analysis of color pixels on the Leonardo painting.

True, the energy flows from large scales. It dissipates at small scales in thin boundary layers of the CVS surface, but this spatial picture is different from the hierarchical cascade of energy "from a big eddy to a smaller one."

The only way to reconcile these two pictures is to assume the Russian doll of nested tubes, passing the energy from the outer tube to the inner ones, with each tube dissipating energy as discussed above. Someone still has to find such a solution of the CVS equations.

The conservation of energy dissipation on the CVS surface makes this parameter \mathcal{E} an appropriate scaling factor for the K41 theory viewed as dimensional analysis.

The K41 energy spectrum undeniably exists at least at medium Reynolds numbers when the vorticity has not yet collapsed into the vortex surface.

Let us come back to our cylindrical solution.

This solution describes a vortex tube much larger than the viscous scale. All vorticity collapses to the boundary layer; this layer's width will decrease as a positive viscosity power in the turbulent limit. The shape of the tube is hyperbolic in each quadrant of the complex plane, with infinite cusps on the real and imaginary axes.

The flow is, therefore, potential both inside and outside. The normal velocity vanishes on both sides of the surface of the tube, but the tangent velocity is finite, and there is a tangent gap (see Fig.12).

Hollow vortex tubes were observed in the recent DNS,¹⁷ but it is hard to tell until some research would specifically hunt for hollow tubes in turbulent flow

simulations.

The uniform strain tensor, distributed as a Gaussian random traceless matrix, is forcing our flow.

The origin of this random force is the accumulation of a large number of $1/R^3$ tails of the Biot-Savart laws for other remote vortex surfaces with random locations and random directions of the net vorticity.

The stability condition, coming from the microscopic analysis of the Navier-Stokes equation in a boundary layer, fixes the sign of the flow.

The same requirement follows from the Kelvin-Helmholtz stability of the vortex surface.

This stability condition $S_{nn} < 0$ is the origin of the flow's irreversibility. We choose the parameters so that the energy dissipation (and equal energy pumping) stays finite in the limit of vanishing viscosity.

We considered these closed vortex surfaces (vortex bubbles) as a dilute gas, with a large mean distance between bubbles, compared to their size.

In this dilute gas approximation, we derived the Gaussian random strain from an infinite number of remote vortex structures, adding to the Biot-Savart formula for the strain at large distances and averaging to the random constant stress tensor due to the Central Limit theorem.

This calculation leads to a self-consistency relation (119) for the variance of the random strain, which then confirms the scaling law¹⁶ for the background strain variance $\sigma \sim \nu^{-\frac{1}{5}}$.

The singular cusps of the hyperbolic vortex sheet lead to multifractal scaling laws for the velocity gap, with the scale R_0 going to zero as some power of viscosity (125), depending upon the ratio $\mu = 1 - \frac{\epsilon}{a}$ of the eigenvalues of the background strain.

The scale R_0 being much smaller than the mean distance \bar{R} between the vortex bubbles vindicates the underlying assumption of an ideal gas of vortex bubbles. The collisions between the thin cusps of our tubes disappear in the turbulent limit.

The statistical distribution of the power index μ in the equation of our surface $|y||x|^\mu = \text{const}$ leads to a distribution (131) of the fractal dimension d of our CVS curve. This distribution offers the microscopic mechanism for the multifractal scaling laws for the moments of velocity difference.

Our estimate (132) provides the mechanism for the multifractal law, although not yet allowing us to compute the anomalous dimension index $\zeta(n)$. Moreover, the moments of velocity difference would likely be a more complex function of $n, |\Delta r|$ than just $|\Delta r|^{\zeta(n)}$, which could be approximated by the power laws at specific integer values of n . This unknown function remains an open problem for future study in the CVS theory.

The SY phenomenological theory¹⁵ relies on the postulate of the renormalized Bernoulli law for local values of pressure in the turbulent flow. We interpret this renormalized law $p = -\frac{1}{2}\alpha\bar{v}^2$ as a probability α to have no vorticity in the point

under study times the local pressure in a potential flow.

The velocity differences in the piecewise potential flow can be singular: with the certain probability of the pair of points are separated by a hyperbolic vortex sheet.

In this case, the pressure obeys the Bernoulli formula on each side. The velocity difference is dominated by the tangent velocity gap, scaling as some power of the size of the CVS surface. The size has a multifractal distribution, which may lead to the desired scaling law.

This topological observation resolves the paradox of singular velocity moments in the potential flow of.¹⁵ With this interpretation, the multifractal law is not exact – it is only an approximation to the future microscopic theory.

Using the dilute gas approximation, we computed the PDF for the energy dissipation in terms of its complex shape form (97), plotted in log-log scale at 13. This curve is universal in our solution; there are no model approximations nor any dimensionless parameters.

In the same way, one can compute the distribution of the circulation and other observables, such as the Wilson loop $\left\langle \exp \left(i \gamma \oint_C v_\alpha dr_\alpha \right) \right\rangle$.

The reader may wonder what the relation between our new vortex sheets and the random surfaces we suggested in¹⁶ is. The CVS surfaces have a deterministic shape up to fluctuating index μ in the equation $yx^\mu = \text{const}$.

The random surfaces of string theory, on the other hand, have local degrees of freedom, fluctuating at every point of the surface. These fluctuations are unstable in three dimensions, so this analogy created a new problem without solving the old one.

As we see it now, the hardest part of the string theory– the random shape of the vortex surface is gone, but some other parts are still relevant.

As it was advocated in,¹⁶ the Gibbs statistics of vortex structures involve soft degrees of freedom on the vortex surface, related to its internal metric. The physical meaning of this internal metric is the transverse motion of the fluid along the surface without changing its shape.

Within the vortex sheet dynamics, such motions lead to re-parametrization of the surface. The conformal metric gives the invariant part of these re-parametrizations, obeying the dynamics of the 2D string theory.^{18,19}

One can describe this metric by a 2D Liouville field, which may be another source of the multifractal scaling laws.

We have to modify this string approach to the Gibbs statistics of the vortex sheets to accommodate the newly found conservation of the anomalous dissipation on the surface.

Acknowledgments

I am grateful to Dennis Sullivan, Theo Drivas, Victor Yakhot, and the Stony Brook University Einstein seminar participants for stimulating discussions of this work. The help from Arthur Migdal with *Mathematica*® is also greatly appreciated.

This work is supported by a Simons Foundation award ID 686282 at NYU.

References

1. J. Burgers, A mathematical model illustrating the theory of turbulence, in *Advances in Applied Mechanics*, eds. R. Von Mises and T. Von Kármán (Elsevier, 1948) pp. 171 – 199.
2. A. A. Townsend, *Proc. Roy. Soc. Lond. Ser. A.* **208(1095)**, 534–542 (1951), doi:10.1098/rspa.1951.0179.
3. A. Migdal, *Physics of Fluids* **33**, 035127 (2021), <https://doi.org/10.1063/5.0044724>, doi:10.1063/5.0044724.
4. K. Shariff and G. E. Elsinga, *Physics of Fluids* **33**, 033611 (2021), <https://doi.org/10.1063/5.0045243>, doi:10.1063/5.0045243.
5. A. Migdal, Confined vortex surface and irreversibility. 1. properties of exact solution (2021), arXiv:2103.02065v10 [physics.flu-dyn].
6. Wikipedia, Double layer (surface science) — Wikipedia, the free encyclopedia (2021), [Online; accessed 24-January-2021].
7. A. Migdal, Algebraic cvs <https://www.wolframcloud.com/obj/sasha.migdal/Published/AlgebraicCVS.nb> (August, 2021).
8. A. Migdal, Hyperbolic flow <https://www.wolframcloud.com/obj/sasha.migdal/Published/HyperbolicFlow.nb> (August, 2021).
9. Wikipedia, Brouwer Fixed-point Theorem https://en.wikipedia.org/wiki/Brouwer_fixed-point_theorem, (2021), [Online; accessed 11-June-2021].
10. A. A. Migdal, Random surfaces and turbulence, in *Proceedings of the International Workshop on Plasma Theory and Nonlinear and Turbulent Processes in Physics, Kiev, April 1987*, ed. V. G. Bar'yakhtar (World Scientific, 1988), p. 460.
11. M. E. Agishtein and A. A. Migdal, *Physica D: Nonlinear Phenomena* **40**, 91 (1989), doi: [https://doi.org/10.1016/0167-2789\(89\)90029-8](https://doi.org/10.1016/0167-2789(89)90029-8).
12. A. Migdal, Matrix integrals <https://www.wolframcloud.com/obj/sasha.migdal/Published/MatrixIntegrals.nb> (May, 2021).
13. A. Migdal, N dimensional tensor algebra and gradients <https://www.wolframcloud.com/obj/sasha.migdal/Published/NDimensionalTensorMath.nb> (Mar, 2021).
14. A. Migdal, *International Journal of Modern Physics A* **35**, 2030018 (November 2020), arXiv:2007.12468v7 [hep-th], doi:10.1142/S0217751X20300185.
15. K. R. Sreenivasan and V. Yakhot, Dynamics of three-dimensional turbulence from navier-stokes equations (2021).
16. A. Migdal, *International Journal of Modern Physics A* **36**, 2150062 (2021), <https://doi.org/10.1142/S0217751X21500627>, doi:10.1142/S0217751X21500627.
17. D. Buaria, A. Pumir, E. Bodenschatz and P. K. Yeung, *New Journal of Physics* **21**, 043004 (Apr 2019), doi:10.1088/1367-2630/abo756.
18. I. Klebanov, String theory in two dimensions (1991), arXiv:hep-th/9108019v2.
19. A. Zamolodchikov and A. Zamolodchikov, *Nuclear Physics B* **477**, 577–605 (Oct 1996),

30

doi:10.1016/0550-3213(96)00351-3.

12. Figures

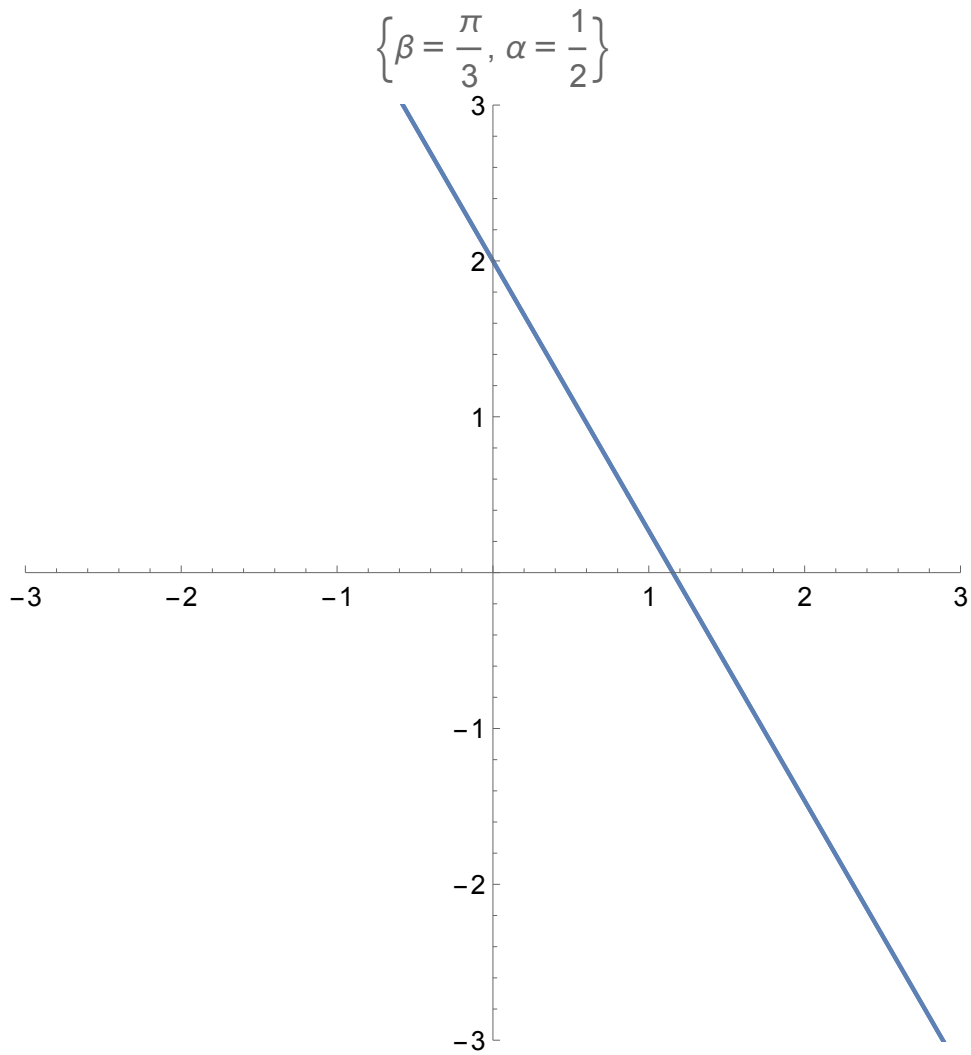


Fig. 1. The Burgers-Townsend case, $n = 0$.

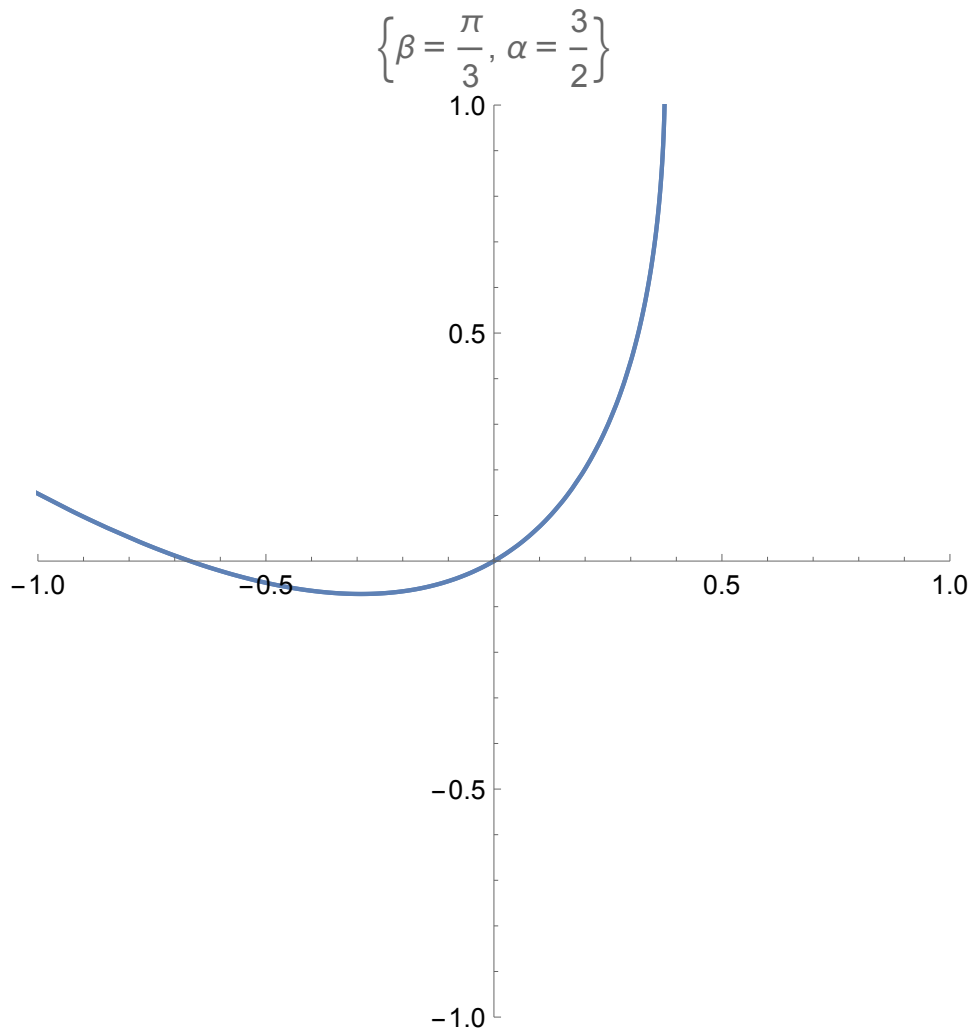
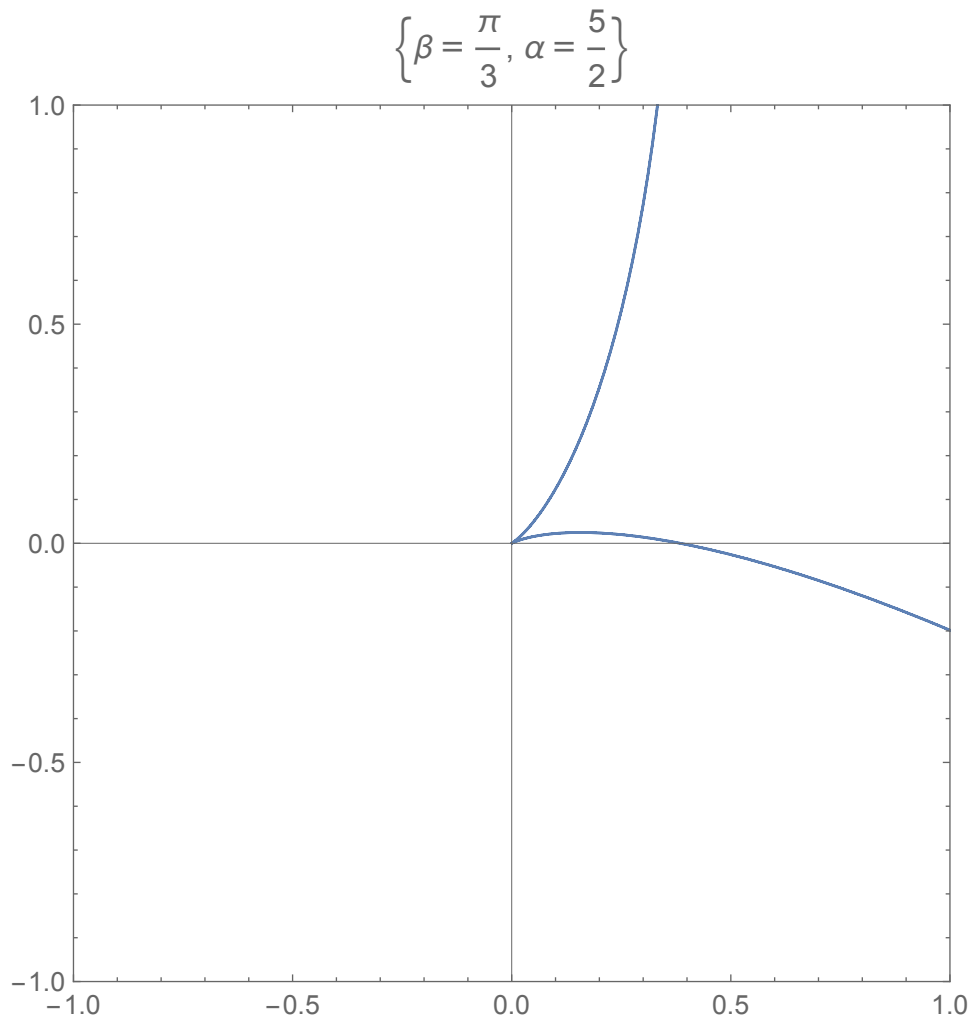
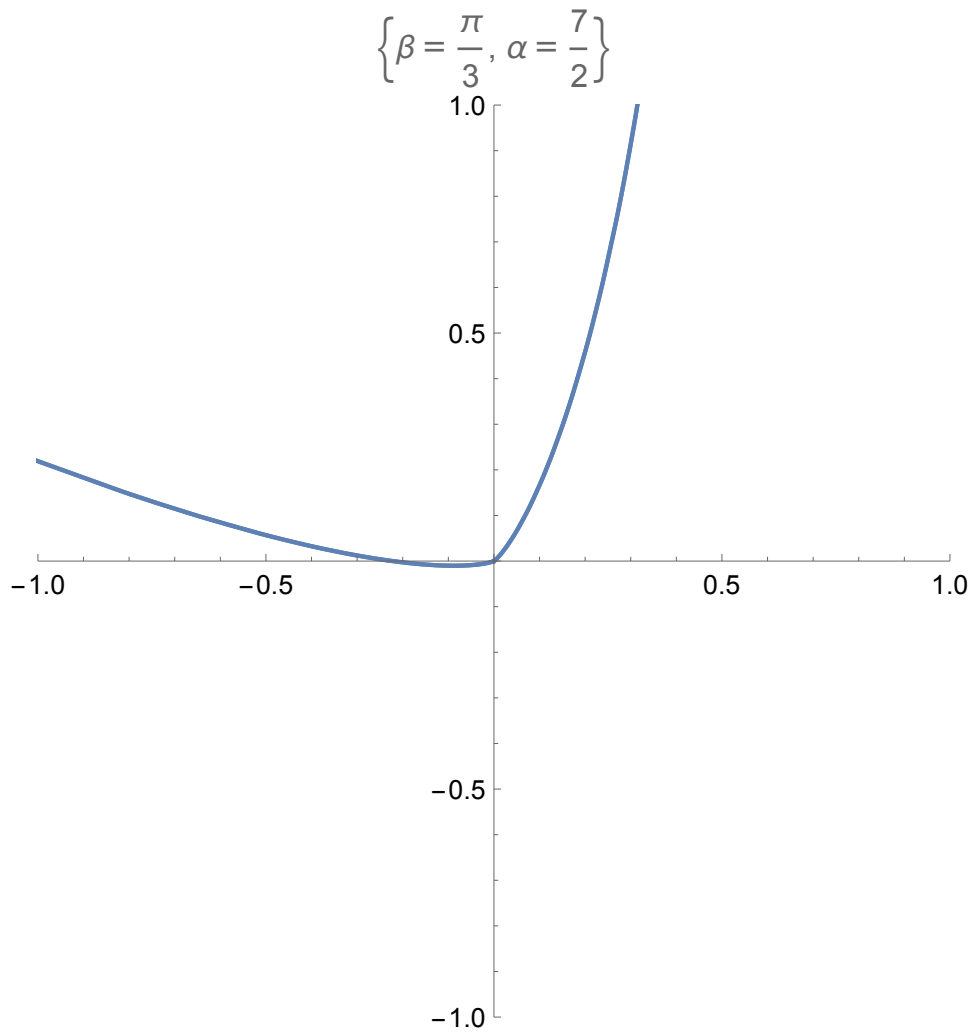


Fig. 2. The CVS for $n = 1$.

Fig. 3. The CVS for $n = 2$.

Fig. 4. The CVS for $n = 3$.

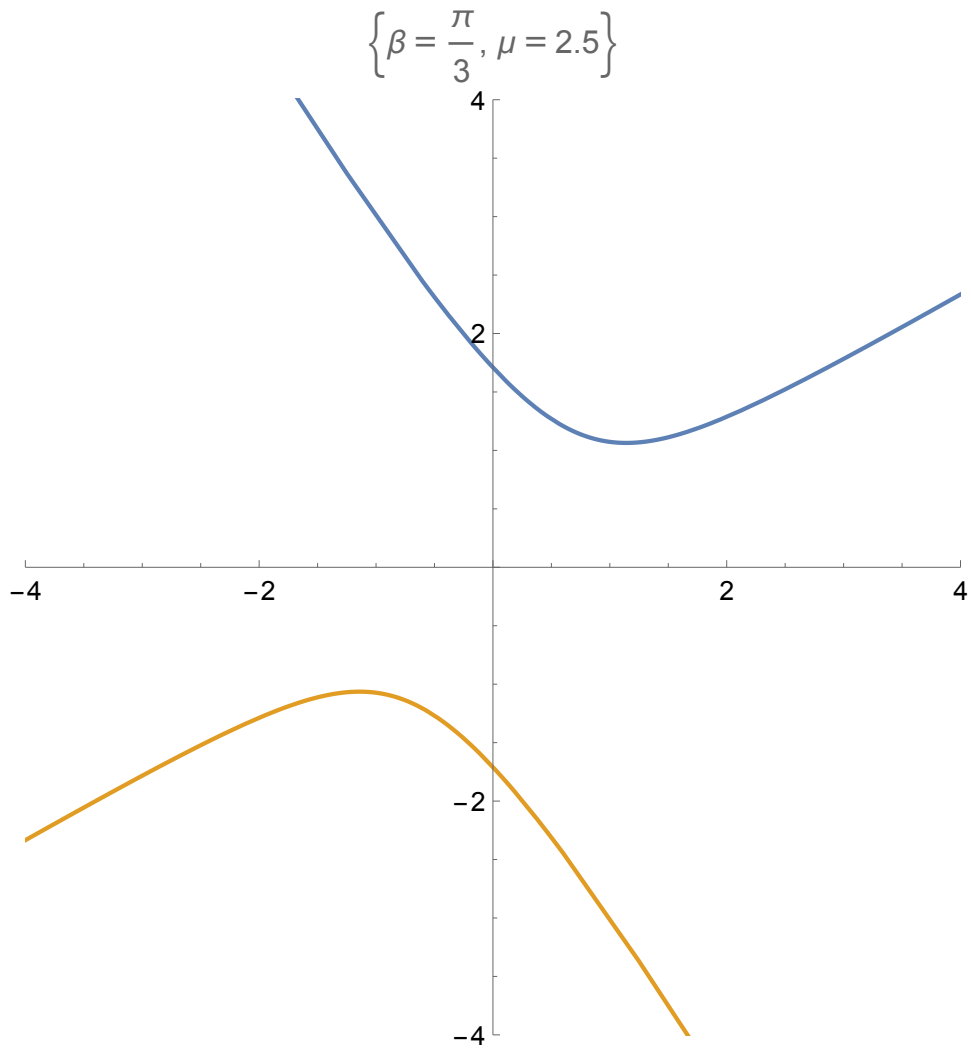


Fig. 5. The hyperbolic CVS for $\beta = \pi/3, \mu = 2.5$.

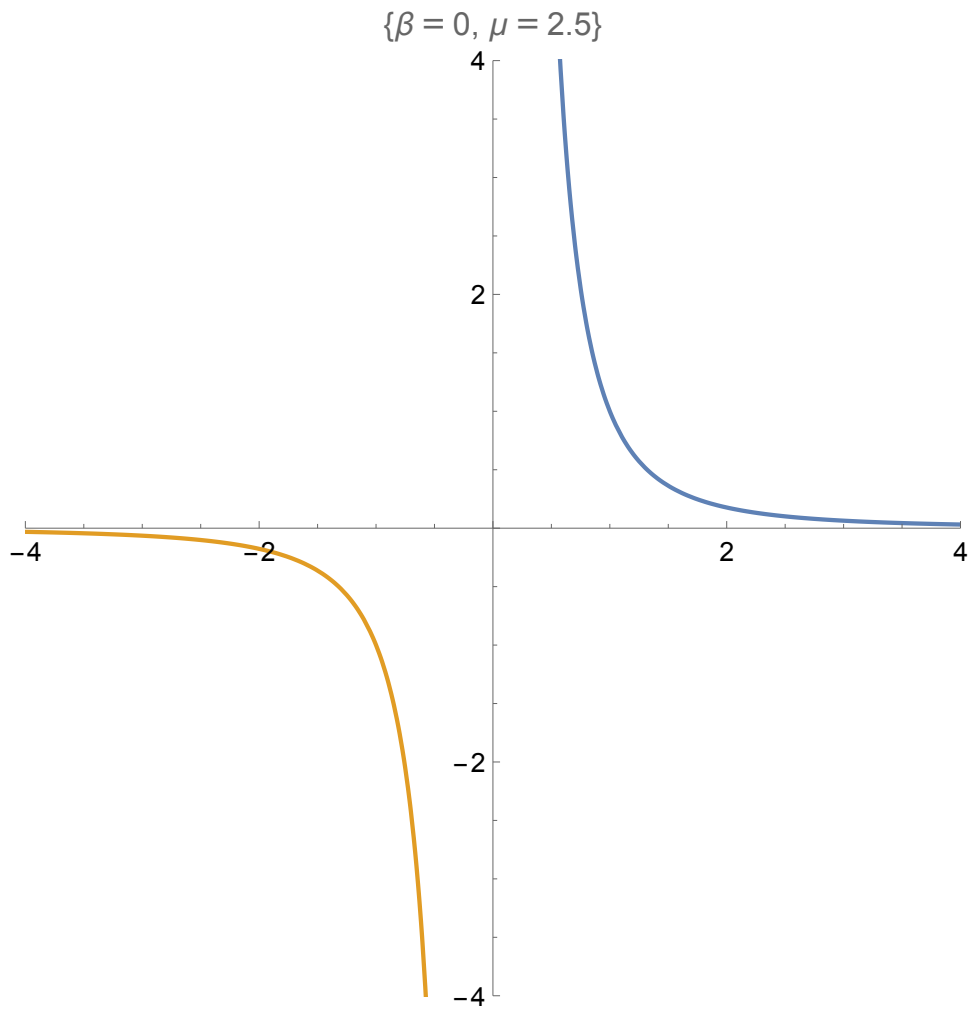


Fig. 6. The hyperbolic CVS for $\beta = 0, \mu = 2.5$

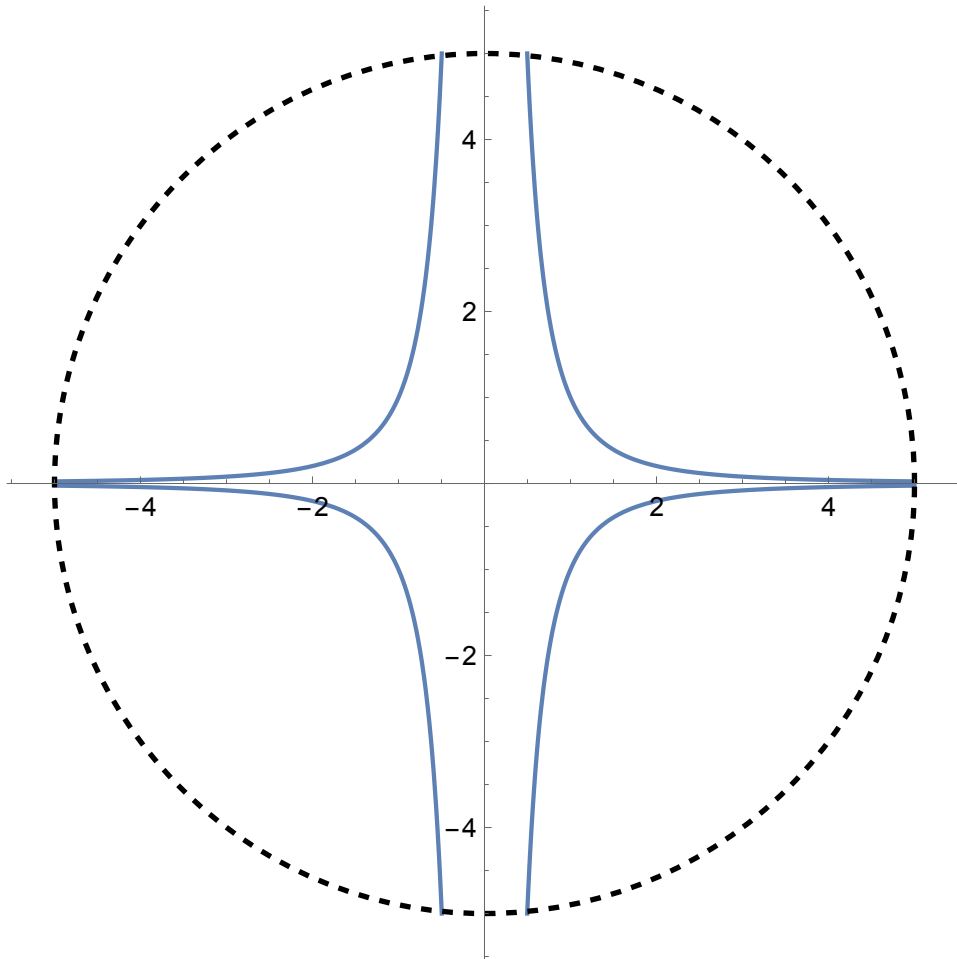


Fig. 7. The loop made of four branches of hyperbola.

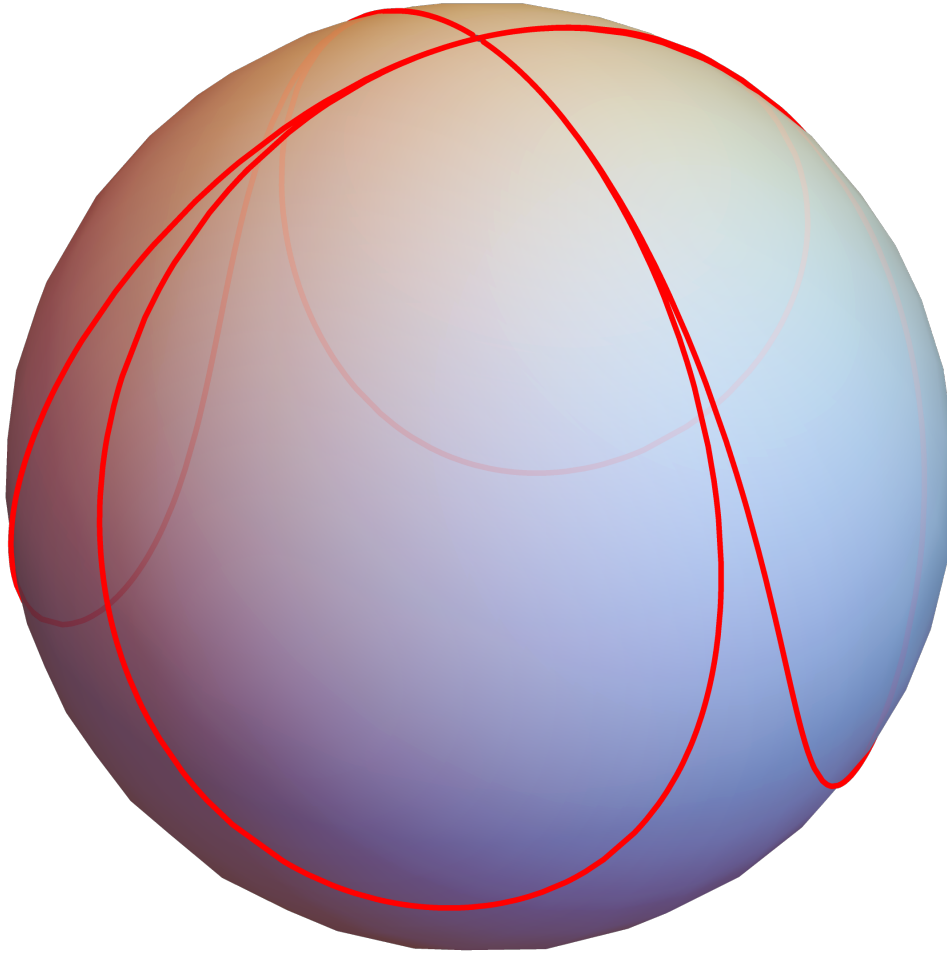


Fig. 8. The stereographic projection of four branches of hyperbola on the Riemann sphere.

$$\eta = 1 + \frac{0.+1.51i}{w^{2.51}}$$

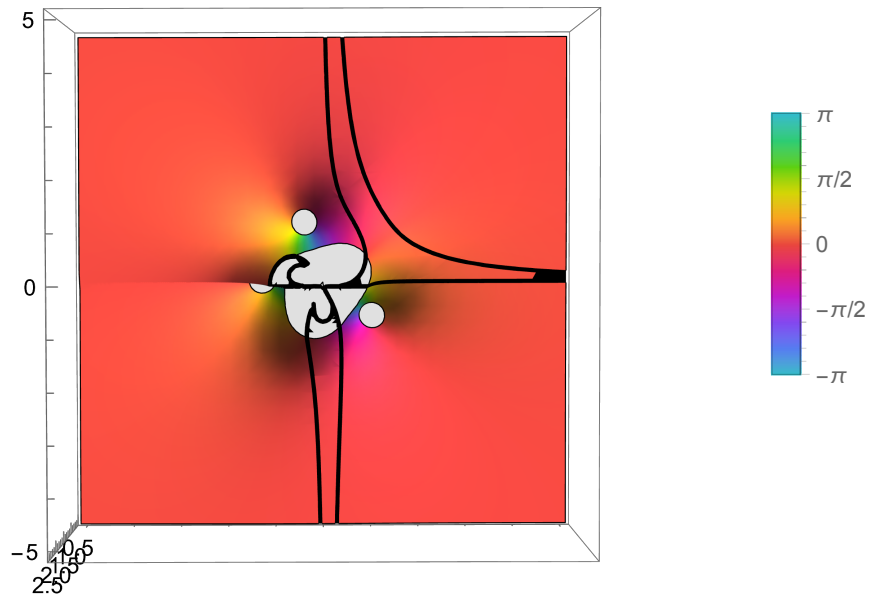


Fig. 9. The complex Map3D of the holomorphic function $\eta'(w) = 1 + i\mu w^{\mu-1}$ for $\mu = 1.51$. The height is $|\eta'|$, the color is $\arg \eta'$. The square root singularities of inverse function $\eta(w)$ is located at the points where $\eta'(w) = 0$. They are indicates as a holes on the surface (white circles). The black lines are described by $(\operatorname{Re} \eta(w))^\mu \operatorname{Im} \eta(w) = \pm 1$. The physical region is outside the black line in the first quadrant, and there are no singularities there.

$$\eta = 1 + \frac{0. + 2.i}{w^3}$$

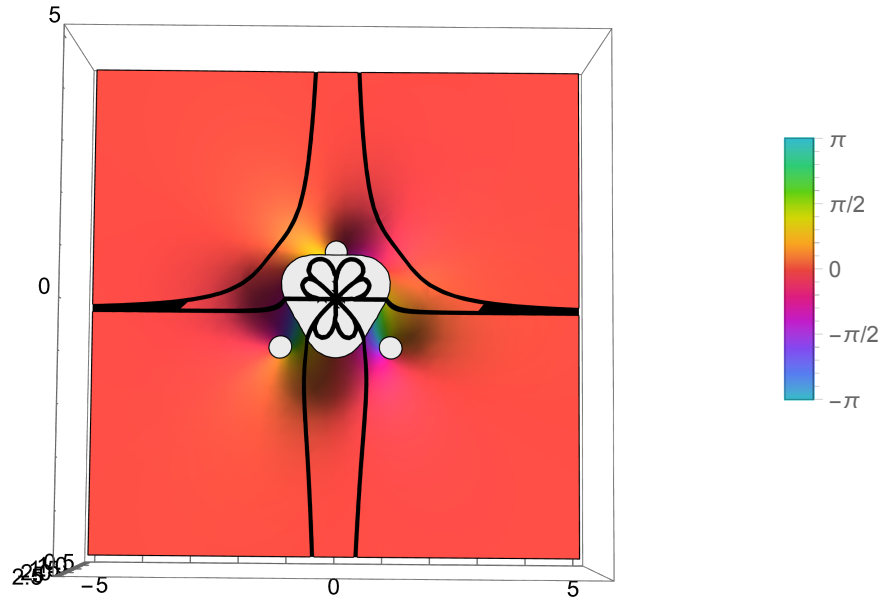


Fig. 10. The complex Map3D of the holomorphic function $\eta'(w) = 1 + i\mu w^{-\mu-1}$ for $\mu = 2$. The height is $|\eta'|$, the color is $\arg \eta'$. The square root singularities of inverse function $\eta(w)$ is located at the points where $\eta'(w) = 0$. They are indicates as a holes on the surface (white circles). The black lines are described by $(\operatorname{Re} \eta(w))^\mu \operatorname{Im} \eta(w) = \pm 1$. The physical region is outside the black line in the first quadrant, and there are no singularities there.

$$\eta = 1 + \frac{0.+2.99i}{w^{3.99}}$$

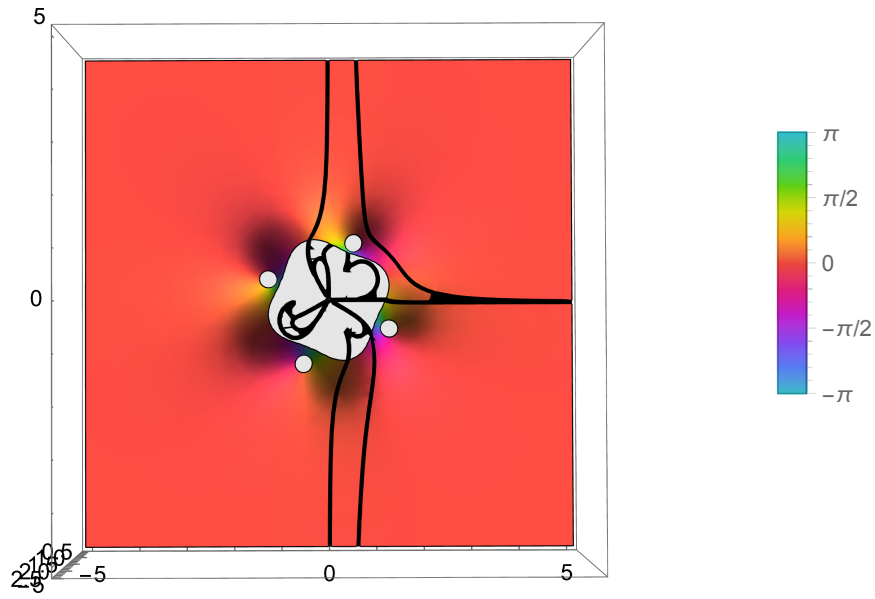


Fig. 11. The complex Map3D of the holomorphic function $\eta'(w) = 1 + i\mu w^{-\mu-1}$ for $\mu = 2.99$. The height is $|\eta'|$, the color is $\arg \eta'$. The square root singularities of inverse function $\eta(w)$ is located at the points where $\eta'(w) = 0$. They are indicates as a holes on the surface (white circles). The black lines are described by $(\mathbf{Re} \eta(w))^\mu \mathbf{Im} \eta(w) = \pm 1$. The physical region is outside the black line in the first quadrant, and there are no singularities there.

$$\{V, \mu = 1.7, v_n \leq 4.32199 \times 10^{-16}\}$$

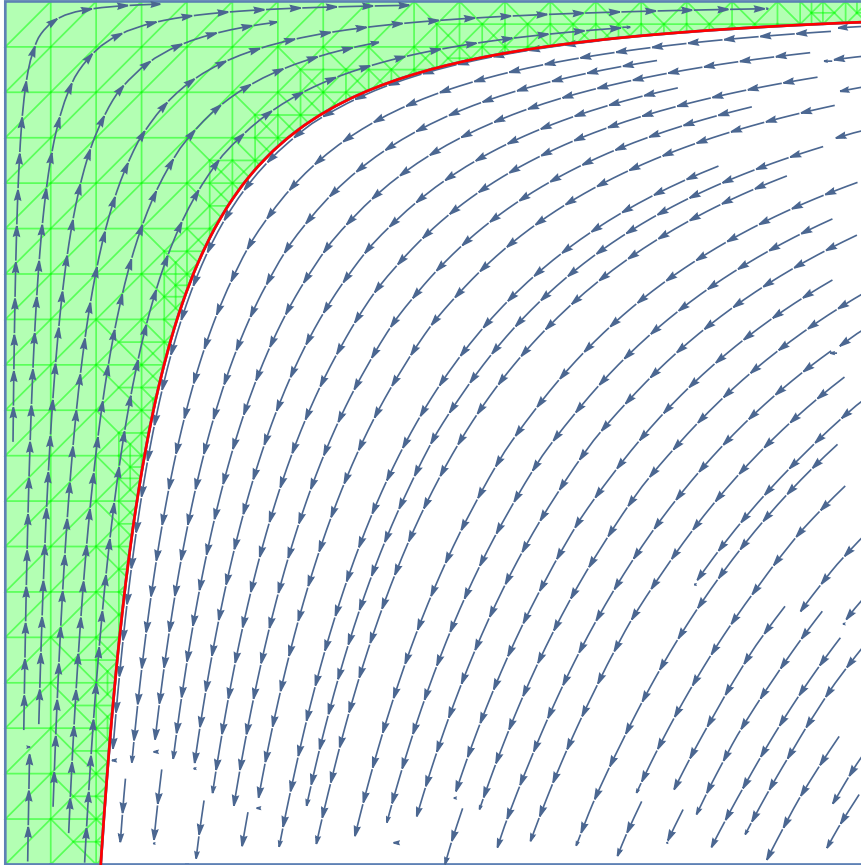


Fig. 12. The stream plot in IV quadrant of xy plane for $\mu = 1.7$. The green fluid is inside, the clear fluid is outside the vortex surface (red). The flow in other quadrants can be obtained by reflection against the x and y axes. The normal velocity vanishes at the vortex sheet on both sides, with accuracy $\sim 10^{-16}$.

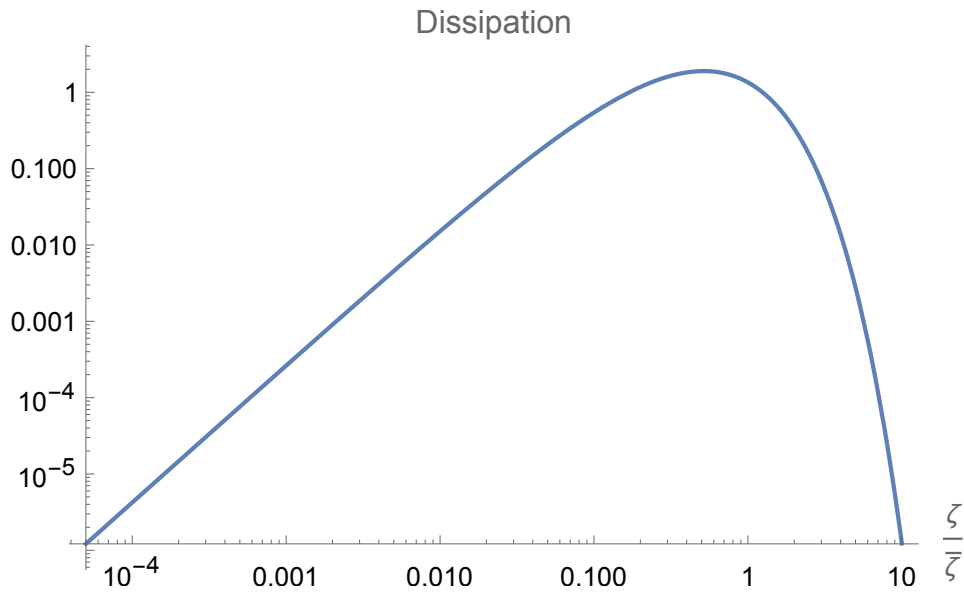


Fig. 13. The energy dissipation PDF in log-log scale

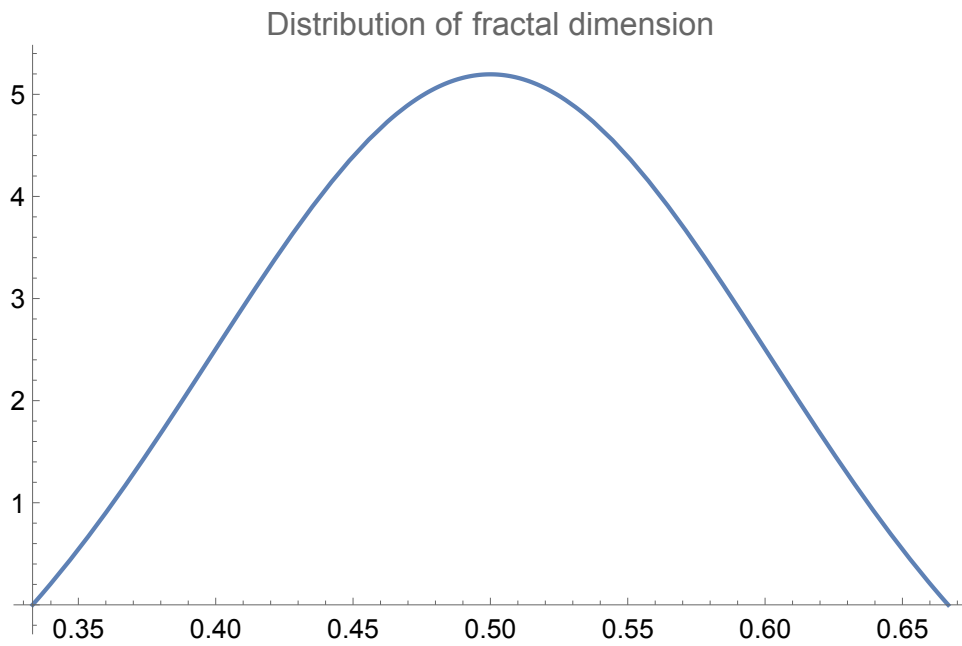


Fig. 14. PDF of fractal dimension of the vortex profile